Aalto University
School of Science

Master's Programme in Mathematics and Operations Research

Optimization of radar and wind farm placement using mixed-integer linear programming

Juuso Varho

Master's Thesis
2025

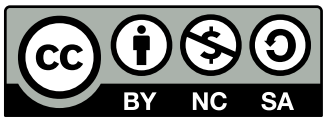

Aalto University
School of Science

Author Juuso Varho

Title Optimization of radar and wind farm placement using mixed-integer linear programming

Degree programme Mathematics and Operations Research

Major Systems and Operations Research

Supervisor Prof. Kai Virtanen

Advisor Prof. Kai Virtanen

Date 26.08.2025 **Number of pages** 72 **Language** English

Abstract

This thesis addresses the coexistence problem of air surveillance radars and wind farms. Wind power is a critical element of the renewable energy transition, for which large wind farms are required to be constructed. However, wind farms cause adverse effects on air surveillance radars and decrease the air surveillance quality. Proper siting of radars and wind farms mitigates these effects and allows for wind farm development while maintaining good air surveillance quality. Currently, limited research exists on the placement optimization of radars and wind farms. Furthermore, the existing methods rely on computationally heavy simulations, which limits the number of placement options for radars and wind farms.

This thesis addresses this gap by developing a method for the joint placement of radars and wind farms using mixed-integer linear programming. This method incorporates models for radar performance and the adverse effects of wind farms. These models are used to calculate system performance measures, which estimate the air surveillance quality of placed radars and wind farms. Two alternative system performance measures are developed, which form the basis for two mixed-integer linear programming formulations. The alternative optimization formulations balance the trade-off between computational complexity and the accuracy of the results, where the less complex formulation converges faster but is not as accurate as the slower and more complex formulation.

The efficiency of the optimization and the feasible scale of the placement problem are analyzed through an example problem with over 10^{100} possible radar and wind farm placement combinations. The example problem is solved with both optimization formulations. The globally optimal solutions of these formulations are obtained in minutes. In the existing literature, no other placement method has been shown to solve the radar and wind farm placement problem at this scale while maintaining global optimality and short runtime.

Keywords air surveillance, mixed-integer linear programming, radar and wind farm coexistence, placement optimization, wind power

Aalto University
School of Science

Tekijä Juuso Varho

Työn nimi Tutkien ja tuulipuistojen sijainnin optimointi käyttäen lineaarista sekalukuohjelmointia

Koulutusohjelma Matematiikka ja operaatiotutkimus

Pääaine Systeemi- ja operaatiotutkimus

Työn valvoja Prof. Kai Virtanen

Työn ohjaaja Prof. Kai Virtanen

Päivämäärä 26.08.2025 **Sivumäärä** 72 **Kieli** englanti

Tiivistelmä

Tässä työssä tarkastellaan ilmavalvontatutkien ja tuulipuistojen yhteensovittamisen ongelmaa. Tuulivoimalla on merkittävä rooli yhteiskunnan siirtymisessä uusiutuviin energiamuotoihin. Tuulivoimaa tuotetaan tuulipuistoilla, jotka koostuvat yksittäisistä tuulimyllyistä. Tuulimyllyt, ja siten myös tuulipuistot, aiheuttavat haittavaikutuksia ilmavalvontatutkille ja heikentävät ilmavalvonnan laatua. Oikeanlaisella tutkien ja tuulipuistojen sijoittamisella on mahdollista minimoida tuulipuistojen haittavaikutuksia, mikä mahdollistaa tuulivoiman kehittämisen sekä korkean ilmavalvonnan laadun ylläpidon. Tutkien ja tuulipuistojen yhteissijoittamista tarkastelevaa tutkimusta on tehty vähän. Olemassa olevat menetelmät perustuvat laskennallisesti raskaisiin simulaatioihin, mikä vähentää vertailtavien sijoittamisvaihtoehtojen lukumäärää.

Tässä työssä kehitetään menetelmä tutkien ja tuulipuistojen sijoittamiseen käyttäen lineaarista sekalukuohjelmointia, jonka avulla on mahdollista optimoida näiden sijainnit, kun sijoitusvaihtoehtoja on paljon. Tämä menetelmä sisältää tutkien suorituskykymallin sekä tuulipuistojen haittavaikutusmallin. Näitä malleja käytetään arvioimaan systeemin, eli tutkien ja tuulipuistojen, suorituskykyä. Työssä esitellään kaksi vaihtoehtoista systeemin suorituskykymittaria, joita käytetään kahdessa sekalukuoptimointimallissa. Toinen optimointimalleista tuottaa tarkempia tuloksia, mutta sen ratkaiseminen on laskennallisesti raskaampaa, kun taas toinen on laskennallisesti vähemmän vaativa, mutta se on epätarkempi.

Kehitetyn menetelmän laskennallista tehokkuutta ja sijoittamisongelman käyttökelpoista kokoluokkaa tarkastellaan esimerkkiongelman avulla. Esimerkkiongelma sisältää yli 10^{100} vaihtoehtoista tutkien ja tuulipuistojen sijoituskombinaatiota. Esimerkki ratkaistaan käyttäen kumpaakin optimointimallia. Näiden mallien globaalisti optimaaliset ratkaisut löydetään minuuteissa. Olemassa olevassa kirjallisuudessa ei ole aiemmin esitelty tässä työssä kehitetyn kaltaista menetelmää, jolla voidaan määrittää tutkien ja tuulipuistojen globaalisti optimaaliset sijainnit lyhyessä ajassa siten, että voidaan ylläpitää korkea ilmavalvonnan laatu ja minimoida tuulipuistoista ilmavalvontaan aiheutuvat haittavaikutukset.

Avainsanat ilmavalvonta, lineaarinen sekalukuohjelmointi, tutkien ja tuulipuistojen yhteiskäyttö, sijaintioptimointi, tuulivoima

Preface

This thesis and my studies at Aalto University have been both a challenging and rewarding journey. This journey would not have been possible without the immense support of many people, to whom I am deeply grateful.

I would like to thank my supervisor and advisor, Professor Kai Virtanen, for his invaluable guidance and feedback throughout my time in the Systems Analysis Laboratory and especially during this thesis. Furthermore, I would like to express my gratitude to my coworkers, who have helped and supported me, as well as making the workdays both lighter and more enjoyable. Thank you also to the individuals at Patria who were involved in this thesis for their input and collaboration.

My deepest thanks go to my partner, whose unwavering patience, love, and belief in me have sustained me throughout my studies. I am equally thankful to my friends for their peer support, encouragement, and the countless memories we have made together. Because of all of you, these years at Aalto University have been some of my happiest and most fulfilling years of my life.

Finally, I owe a profound debt of gratitude to my family, who have always supported my education and encouraged me to pursue my ambitions. From setting me on this path to cheering me on at every step, your belief in me has been the foundation on which all of this has been built.

Otaniemi, 26.08.2025

Juuso O. Varho

Contents

Abbreviations

AESA	Active electronically scanned array
ASR	Air surveillance requirement
EU	European Union
GCS	Geographic coordinate system
LOS	Line of sight
MILP	Mixed-integer linear programming
RaPM	Radar performance measure
RCS	Radar cross-section
SNR	Signal-to-noise ratio

1 Introduction

Wind energy production plays a critical role in the transition to clean and sustainable energy systems. In recent years, the global wind power capacity has increased rapidly and is estimated to keep steadily increasing in the coming decades (Costanzo et al., 2025). Wind power is emissions-free, and after installation, the generation of electricity is practically free. However, despite these environmental and economic benefits, wind power development comes with downsides caused by the wind farms. The local communities living near wind farms are affected by their noise and perceived visual degradation of the landscape (Saidur et al., 2011). Most of these problems can be reduced or resolved with proper siting. However, the siting of wind farms is made additionally difficult due to wind farms causing adverse effects on air surveillance.

Air surveillance is the systematic monitoring of airspace to detect and track flying objects, e.g., aircraft and missiles (Merriam-Webster, n.d.). This monitoring is mainly performed with air surveillance radars. Wind farms pose a significant challenge to the air surveillance radars. The wind farms can obstruct a radar's line of sight, reducing the ability to detect and track targets in the affected area (Theil et al., 2010). Moreover, the wind farms reflect radar signals back towards the radar, which causes clutter, i.e., unwanted noise, in the radar image (Theil et al., 2010). The reflected radar signal can be falsely interpreted as an aircraft, which can trigger unnecessary operational responses by air surveillance authorities. These effects cause the wind farms to decrease the overall air surveillance quality, meaning how well the radars are able to detect and track targets in the surveillance area. The siting of both wind farms and radars directly affects the air surveillance quality and the severity of the adverse effects. The conflicting objectives of maintaining good air surveillance quality and increasing wind power generation cause a coexistence problem between the objectives.

The urgency of resolving this issue is highlighted by the European Union's (EU) ambitious energy goals. The EU has committed to doubling the share of renewables in its energy consumption and to quadrupling the annual wind power generation by 2030 (European Commission, 2023). Achieving these targets requires the rapid deployment of new wind energy projects. However, the permitting process remains a significant bottleneck, as it requires approval from multiple national authorities and is criticized to be slow and complex (European Commission, 2023). One of these authorities is the air surveillance authority, who are in charge of maintaining high air surveillance quality. If a proposed wind farm decreases the surveillance quality significantly, the plan must be rejected for national security reasons. Due to the detailed analysis of air surveillance quality being classified information, there is limited transparency and communication for specific wind farm rejection reasons. This limited transparency and communication are deemed problematic by the wind farm developers (Joensuu et al., 2021). For instance, the challenges in the permitting process and concerns over air surveillance quality are among the reasons for limited wind power development in Eastern Finland (see, e.g., Peiponen, 2022; Pelli, 2023).

To achieve the ambitious EU-level goals for wind power generation, the permission process needs to be accelerated. One potential approach could be to let the wind farm developers to determine possible locations for wind farms, and then letting the

national permitting authorities to decide the most suitable sites for their development. In this approach, the surveillance authorities would also determine a corresponding set of viable radar sites. These predefined options could then be jointly analyzed to determine the optimal placement of both radars and wind farms. This approach is additionally reasonable as some radars are designed to be movable (Keränen, 2020).

Despite the importance and urgency of developing ways to accelerate the permission process, limited research is available on the optimization of radar and wind farm placements. The prior literature is mostly focused on optimizing the radar or wind farm placement in isolation (see, e.g., Roy and Acharya, 2017; Cranmer et al., 2018). The existing methods on the joint placement optimization of radars and wind farms (see, e.g., Lahti, 2022; Hagnäs, 2025) are dependent on computationally heavy simulations, and are thus limited to only consider a small number of placement options. These existing methods for the radar and wind farm placements are discussed further in Section 2.4. No literature exists on optimizing these placements from a large number of placement options. This gap highlights the need for a method for efficient evaluation of radar and wind farm placements and for placement optimization.

This thesis addresses the limitation of existing radar and wind farm placement methods, which can only consider a small number of placement options, by developing a new method for their joint placement. This method consists of a radar performance model, which estimates the radar's ability to detect and track targets, and a wind farm adverse effect model, which estimates how the radar performance is degraded due to wind farm interference. With these models, the air surveillance quality of placed radars and wind farms is estimated with two alternative system performance measures. The 3D-system performance measure estimates the air surveillance quality in individual 3D-locations, which is more accurate and computationally more complex. The 2D-system performance measure estimates the altitude-wise aggregated air surveillance quality, which decreases the computational complexity, with the cost of decreased accuracy of the results. These system performance measures are used for two alternative mixed-integer linear programming (MILP) formulations: 2D and 3D. These formulations use the radar and wind farm placements as decision variables and their objective function is to maximize the air surveillance quality in the whole area of interest. Two formulations are constructed to address the trade-off between the computational complexity of the optimization and the accuracy of the results. As the 3D-formulation uses the more accurate 3D-system performance measure, it is computationally more complex and the optimization takes longer to converge. The 2D-formulation uses the simplified 2D-system performance measure, which makes the optimization faster but decreases the accuracy of the performance models.

With the method developed in this thesis, the radar and wind farm placements, which maximize the air surveillance quality, are able to be identified from large number of placements options. The set of viable placement options is determined by their corresponding planners and is out of scope for this thesis. The method enables the air surveillance planners to identify the optimal locations for radars and wind farms and to efficiently model the resulting adverse effects. The method also allows the surveillance planners to consider the varying importance of different spatial areas and altitudes. These importance differences are taken into consideration with weighting, where the

high air surveillance quality can be prioritized in different spatial areas and altitudes. This method is also modular, meaning the radar performance model, the adverse effect model, and the optimization formulations can be modified without altering the whole method. This modularity allows for easy modification of the underlying models, allowing them to be updated or extended in later work.

The efficiency of the placement method and the feasible scale of placement problems are analyzed with an example problem. The example considers the placement of radars and wind farms with a large number of placement options. The impact of weighting is demonstrated by applying both uniform and non-uniform weights across spatial areas and altitudes. The example is solved with both optimization formulations to analyze the differences in the optimal placements. The example problem is purely hypothetical and is intended solely to analyze and demonstrate the placement method developed in this thesis.

No other method has been shown to solve the radar and wind farm placement problem with as many placement options while maintaining global optimality and short runtime. The existing methods for radar and wind farm placement optimization rely on computationally heavy simulations to estimate the air surveillance quality, which limits the number of placement options they can evaluate. The method developed in this thesis allows for the identification of good placement sites for radars and wind farms from large number of placement options. However, as the method uses a simplified measure of air surveillance quality, its accuracy is limited. Therefore, this method is suitable for identifying good candidate sites, which can then be further evaluated using more detailed and accurate simulation approaches.

Air surveillance systems and the adverse effects of wind farms on radars are discussed in more detail in Section 2, detailing factors affecting the air surveillance quality and its evaluation. The placement method is introduced in Section 3, outlining the radar performance model, the wind farm adverse effect models, and the two system performance measures. The two alternative optimization formulations are constructed in Section 3.3 based on the system performance measures, and their differences are discussed. The feasible problem scale and the results of the method are demonstrated with an example problem in Section 4. Finally, the method and the example problem solutions are discussed further in Section 5, and the thesis is summarized in Section 6.

2 Coexistence of air surveillance systems and wind farms

This section provides an overview of air surveillance systems and methods used to evaluate their performance. Then, the adverse effects of wind farms on a radar's operation and the overall air surveillance quality are discussed. Finally, the approaches for placement planning of radar and wind farms are discussed, which aim to maintain high air surveillance quality and minimize the adverse effects of the wind farms.

2.1 Air surveillance systems

Air surveillance is a critical component of defense and civil aviation safety, consisting of monitoring the airspace with a variety of sensors. The primary objective of the monitoring is to detect the use of the airspace, create situational awareness, and support decision-making in areas such as air traffic control and military threat assessment (Finnish Air Force, n.d.). In military applications, decision-making is guided by the airspace operational picture, which forms the basis for all air operations (Finnish Air Force, n.d.). This operational picture is formed from all the available airspace information, which is mainly collected by an air surveillance system. The accuracy and reliability of this picture depend on the performance of the air surveillance system.

An air surveillance system consists of a wide variety of sensors used to detect the airspace, and a tracker used for estimating a target's track. This track refers to the continuous monitoring and updating of a target's position, velocity, and flight direction over time as it moves through airspace (Richards et al., 2010). The tracker forms a track estimate by fusing data from various air surveillance sensors. The foundation of these sensors are radars. A radar is an electronic system that emits a radio signal towards the region of interest and detects the signals reflected from an object in that region (Richards et al., 2010).

The ability of an air surveillance system to detect and track a target is greatly affected by the strength of the reflected radar signal. The amount of radar signal reflected back by the target is determined by its radar cross-section (RCS). The RCS depends on a variety of factors, such as the position of the radar relative to the target, the target's shape and material composition, and its orientation relative to the radar (Knott et al., 2004). An object with a larger RCS is more easily detected than one with a smaller RCS. As the RCS directly affects how easily the target is detected, stealth technology has emerged to minimize the RCS and to avoid radar detection (Richards et al., 2010). The RSC is most effectively reduced by using radar-absorbent materials and designing the target's geometry to minimize direct reflections (Zohuri, 2020). Due to the emergence of stealth technology, the performance of radars is made additionally important.

The performance of the radar system is fundamentally determined by how effectively the combination of the radars is able to detect and track objects within the set area of interest. This capability depends on the types of radars used, their geographic placement, and the performance capabilities of the individual radars.

One of the most commonly used sensor is the monostatic radar, which is a radar type where the signal transmitter and receiver are in the same location. This radar type is prevalent for its simplicity and efficiency in deployment, as it can be deployed and moved easily (Finnish Air Force, n.d.). However, these types of radars can be vulnerable to electronic countermeasures, such as jamming, and have limited effectiveness against stealth technology, which minimizes direct radar reflections towards the emitter (Chemyak, 1998). To address these limitations, in bistatic radars, the transmitter and receiver are in different locations. This radar type can be more effective against stealth technology, as the reflected radar signal may still reach a receiver positioned elsewhere. This design can be further improved by using multiple spatially separated transmitters and receivers, or a collection of monostatic radars, referred to as multistatic radar systems (Chemyak, 1998). The detection and tracking capabilities of a multistatic radar system are improved due to cooperative performance and interaction between the individual radars.

While the performance of the radar system is improved with cooperative sensing, the overall effectiveness of the radars is determined by their individual capabilities. The capability of a radar is described by its parameters, such as range resolution, scan rate. A radar's contribution to the air surveillance quality, i.e., how well the radar system can detect and track target objects, is dependent on these individual parameters. The range refers to the maximum distance at which the radar can detect an object with the specified RCS. The range is dependent on radar's parameters, such as the transmitter power and antenna gain, which describes how narrowly the radar beam is focused in a particular direction, and the target's RCS (Skolnik et al., 1980). The radar range is further affected by the environmental conditions, such as weather, humidity, and terrain, which can absorb, scatter, or block radar signals. However, the emitted radar signal can continue further than the estimated range, meaning some surveillance capability is possible outside the reported range. The resolution describes the radar's ability to distinguish between multiple closely spaced objects. The resolution consists of range resolution, meaning the ability to distinguish targets at the same direction but at different distances, and angular resolution, meaning the ability to distinguish targets at similar distances but at different angles (Richards et al., 2010). High resolution is important for accurate target tracking and enhances the detail and clarity in the operational picture. According to Skolnik et al. (1980), with sufficiently high resolution, the nature of a target's size and shape can be discerned. The size and shape estimations are additionally useful in trying to identify the detected targets. A high resolution is typically achieved with a higher frequency radar signal, which comes with a trade-off in radar range, as longer ranges are more easily achieved with lower frequencies (Skolnik et al., 1980). The scan rate refers to how frequently a radar completes a full sweep of the area of interest, and directly affects how frequently the radar can detect and estimate target position.

In summary, the real-world air surveillance systems consist of a variety of sensors to monitor the airspace. In this thesis, the air surveillance system is considered to only consist of monostatic radars. The effectiveness of such a system is dependent on the individual performance characteristics of the radars and their spatial placement. The planning of air surveillance systems and the comparison between these different

systems requires methods to systematically evaluate the performance against possible targets.

2.2 Performance evaluation of air surveillance systems

To evaluate the performance of an air surveillance system and compare different systems, analytical models are required to compute performance metrics, which measure a system's ability to detect and track targets. These models vary in complexity and accuracy. The performance can be estimated using simplified calculations that assume idealized conditions and static parameters, or with computationally complex simulations, which can model target behavior, sensor fusion, and environmental conditions and effects (Curry, 2004). However, higher complexity does not mean better system representation. Curry (2004) further states that the performance measures are required to be simple enough to allow for large-scale system simulations and to be able to represent radars whose detailed design is not fully known.

A simplified approach to modeling radar performance is coverage analysis. The coverage can be modeled as either all-or-nothing or gradual coverage. The all-or-nothing model, also known as a boolean coverage model, considers coverage to be binary, meaning a location can either be fully covered or not at all (Wang, 2010). This type of coverage model has been used, e.g., in determining the locations a radar can see, and this information is used in placing radars (see e.g., Baek et al., 2014). In contrast, the gradual coverage model (Drezner et al., 2004) relaxes this binary representation by allowing the amount coverage to vary continuously, i.e., a location can also be only partially covered. In radar performance modeling, this partial coverage can be used to describe the diminishing radar signal strength with increasing range. Therefore, the radar coverage can be higher in some locations than others, indicating higher radar performance. When multiple radars are involved, the coverage at a given location can be defined as a function of the individual gradual coverage values, which can be used to represent sensor fusion. Environmental constraints, such as terrain obstructing the line of sight (LOS), can also be included in the coverage analysis to reflect real-world limitations. An in-depth review on general coverage analysis can be found in Berman et al. (2010), and detailed discussion on sensor coverage models is given in Wang (2010).

The coverage analysis does not take into account the probabilistic nature of target detection. To address this, a more refined metric, the probability of detection is used. This metric quantifies the likelihood that a target is detected by taking into account factors such as range, target RCS, clutter, and atmospheric attenuation (Richards et al., 2010). The probability of detection is largely dependent on the strength of the reflected signal compared to the background noise, referred to as the signal-to-noise ratio (SNR). To detect the target with a reasonable probability, the reflected signal must be greater than the noise (Richards et al., 2010). If the background noise is static, a constant detection threshold level can be set, where SNR larger than the threshold is interpreted as a detection. In modern radars, this threshold is adjusted automatically based on the noise level due to, e.g., jamming or clutter. The threshold is adjusted such that inferences result in a constant false alarm rate, which directly affects the

probability of detection (Richards et al., 2010). Increasing the constant false alarm rate will increase the probability of detecting a target, but also increases the probability of false alarms, meaning detecting a target even though it does not exist (Richards et al., 2010). The probability of detection is further improved when the coverage of multiple radars overlaps. This improvement is achieved through sensor fusion, which combines the reflected signals from multiple radars to produce a single and more accurate detection probability (Olivier et al., 2009). The probability of detection is additionally improved with a multistatic system design, where the emitted radar signal from one radar can be detected in another (Chemyak, 1998).

After a target is detected, an air surveillance system needs to be able to track and estimate its movements. The tracking performance is measured with the probability of forming a track and the error between the estimated track and the true flight path (Ruotsalainen & Jylhä, 2017). The track performance is affected by the target RCS, the probability of detection, the accuracy of the target's position estimation, and how frequently the target position is updated. Hence, the track performance is dependent on the individual radar characteristics, such as resolution and scan rate. The tracking performance of an air surveillance system is typically calculated by simulating multiple flight paths and estimating the track and determining its error, which is computationally intensive (Ruotsalainen & Jylhä, 2017).

While each of the metrics discussed above provides insight into the radar system performance, the metrics by themselves do not provide a complete picture of the overall quality of air surveillance. In Virtanen (2024), a spatial multi-criteria decision analysis framework is developed for the evaluation of air surveillance quality. In this framework, the different objectives in the surveillance area, such as target detection and tracking, are described by air surveillance tasks. These tasks are formalized into air surveillance requirements (ASRs), which are defined by a 3D surveillance area, a target type, quality statements of performance measures, and a priority. The target type refers to the characteristics of a target aircraft, such as its speed and RCS. With the ASRs, a decision maker can prioritize different performance measures or spatial areas to reflect possible air surveillance needs and tasks. Different measures are developed to measure the fulfillment of the ASRs. This fulfillment of ASRs can be used to evaluate the performance of an air surveillance system and to compare different surveillance systems.

The various performance measures discussed previously enable the assessment of air surveillance systems in target detection and tracking. In addition to the evaluation and comparison of different surveillance systems, these measures can also be used to analyze how external factors, such as infrastructure, may degrade the air surveillance quality. One of these factors is wind farms, which are known to cause adverse effects on radars. Assessing the magnitude of these effects is essential when considering the placement and development of new wind farms or the placement of radars.

2.3 Adverse effects of wind farms

A wind farm is a collection of wind turbines that are close to each other and are used to produce electricity. The geographical placement of wind farms is critical

to the financial success of the wind farm in terms of installation costs and future profits. Wind farm sites are typically chosen based on wind conditions, terrain and environmental conditions, as well as distance to electricity transmission lines and infrastructure (Wimhurst et al., 2023).

In contrast to the wind farm's financial success, wind farms can interfere with radar and reduce their air surveillance quality. This interference is directly affected by the geographical placement of the wind farms and radars. A wind farm placed within a radar's LOS reflects and disperses the radar signal, diminishing the radar's capability to detect targets. The wind farm can reflect the radio signal back to the radar, and this radar echo causes clutter to appear near the wind farm. Typically, Doppler processing is used to distinguish moving targets from clutter caused by static objects or terrain (Capraro et al., 2006). However, the moving turbine blades in the wind farm provide a significant Doppler profile, which means the clutter can not be removed with Doppler processing (e.g., Theil et al., 2010; Norin and Haase, 2012). Theil et al. (2010) also mentions that the Doppler profile of a single wind turbine echo resembles the profile of a helicopter, meaning the wind farm causes false targets in its vicinity. This increase in false targets means the target detection threshold is increased to maintain a constant false alarm rate, which reduces target detection sensitivity around the wind farm (Borely, 2014). For some radars, these clutter effects can be observed tens of kilometers away from the wind farm (Norin & Haase, 2012).

In addition to the clutter, wind farms also cause shadowing effects, which result from the obstruction and scattering of the radar signal. Unlike the clutter effect, the shadowing primarily affects the area behind the wind farm from the radar's perspective (Lemmon et al., 2008). This is referred to as the shadowing area. Due to the shadowing effects, the radar signal is weaker in the shadowing area, which decreases the performance of the radar. Typically, the shadowing effect decreases as the distance between the radar and the wind farm increases due to diffraction, which bends the radar signal around the wind farm (Theil et al., 2010).

The severity of the clutter and the shadowing effect depends on the orientations of the wind farm turbines, specifically the nacelle and blade orientations (Lemmon et al., 2008). The effects are maximized when the RCS of the blades is maximized, which occurs when the turbine blades face the radar directly, i.e., when their surface is perpendicular to the radar's LOS. As discussed in Lemmon et al. (2008), because all the relevant wind farm parameters are not known, it reasonable to use conservative assumptions in modeling the adverse effects to not underestimate the potential impacts of the wind farms. In this thesis, the wind farms are conservatively assumed to always be oriented towards a radar, such that the potential adverse effects are maximized.

The clutter and shadowing effects can also be observed even when the LOS of a radar only passes near the wind farm and not through it. This occurrence is due to the radar beamwidth and the Fresnel zone of radio signals (Pertilä et al., 2023). Radar beams have both horizontal and vertical widths, meaning the transmitted energy is not confined to only a narrow line but rather spreads out. As a result, objects located near the LOS can reflect the radar energy, causing clutter. Therefore, clutter can occur even when the radar LOS does not pass through the wind farm. Similarly, the shadowing effect can also be observed in an area where the radar's LOS does not pass through the

wind farm. This phenomenon is due to the wind farm disrupting the Fresnel zone of the radar signal, which can lead to destructive interference of the radar signal, reducing the radar performance (Freeman, 2007). The magnitude of this effect is dependent on how much of the Fresnel zone is obstructed, such that the effect decreases when the distance between the LOS and the wind farm increases.

2.4 Placement planning of radar systems and wind farms

As explained in Section 2.1, the air surveillance quality is dependent on what type of radars are being used. However, this quality is also highly dependent on the placement of those radars. The radar placement directly affects the radar's coverage as the placement determines whether the LOS is obstructed by the terrain, e.g., by hills. Elevated locations are typically preferred to minimize the effects of terrain and to extend the radar's horizon. However, determining the radar placements that maximize the air surveillance quality is a complex problem. The placement problem can be formulated into an optimization problem with integer programming, where the goal is to identify the optimal radar placements with regard to some optimization criteria, such as air surveillance quality. In this formulation, the radar placements are represented as decision variables, which can have either value 1 if the placement is used or 0 if it is not. This optimization problem is proven to be NP-hard (Godrich et al., 2011). The NP-hardness means that the search for the optimal radar placement becomes rapidly computationally demanding as the number of placement options increases. For more detailed discussion on NP-hardness, see, e.g., Garey and Johnson (1979).

Because the integer programming formulation of the radar placement problem is NP-hard, it has previously been solved with metaheuristic search methods. These metaheuristic methods work by guiding the candidate solutions through the solution space – i.e., the set of possible placement combinations – with a problem-specific heuristic to find optimal or near-optimal solutions (Blum & Roli, 2003). One metaheuristic search method is the evolutionary algorithm (Simon, 2013), which evolves a candidate solution towards better solutions. Additionally, the evolutionary algorithms can be used to optimize the radar placements while considering multiple criteria. For example, Boudjemaa and Oliva (2019) optimized a weather radar network placement, while considering criteria such as terrain, radar beam elevation, distance between radars, and distance between power grids and roads. Similarly, Roy and Acharya (2017) determined optimal weather radar locations with multiple criteria by using another metaheuristic method, particle swarm optimization. In particle swarm optimization, a swarm of particles – i.e., multiple candidate solutions – is initialized in different positions within the solution space in parallel. These particles are then guided towards better solutions based on their own previous best position as well as the best positions of the other particles in the swarm (Kennedy & Eberhart, 1995). These metaheuristic search methods are efficient in exploring large solution spaces and providing good solutions in a reduced amount of time (Blum & Roli, 2003). However, these methods have no guarantees of the optimality of the result.

To guarantee global optimality, the integer programming formulation of the placement problem needs to be solved with an exact algorithm. While exact algorithms

exist for non-linear formulations, they are more computationally demanding to optimize than linear formulations (Hochbaum, 2007). Due to integer programming problems being NP-hard, linear formulations are typically more practical and remain feasible with a higher number of placement options. The placement problem can be formulated with integer linear programming, where the decision variables are restricted to be integers, and the objective function and the constraints are linear. This integer linear programming problem can then be optimized using an exact algorithm, such as the branch-and-bound (He et al., 2014) or the simplex method (e.g., Padberg, 2013). For example, in Baek et al. (2014), the coverage of radars is described using the boolean coverage model, and the radar placement problem is formulated using integer linear programming. With this formulation, the radar placements, which globally maximize the radar coverage, are able to be identified. However, the real-world performance of radars is not binary, as radars can have varying performance levels, and the performance can be improved with overlapping radar coverage. This varying performance can be modeled with mixed-integer linear programming (MILP) by including non-discrete decision variables. For example, Tanergüçlü et al. (2012) determines the optimal placement of weapons systems, such that the possible flight route of enemy aircraft has maximal expected coverage by the weapon system. The MILP formulation allows for the coverage to have a non-discrete value representing the probability of target detection. Using exact algorithms to solve these integer and mixed-integer linear programming formulations ensures that the placements are globally optimal and the coverage is maximized.

The optimal placement is not only important for radars but also a key consideration for wind farms. As stated by Costanzo et al. (2025), the number of wind farms is predicted to increase rapidly. The placement of these new wind farms requires a careful balance between maximizing energy generation potential as well as other technical, economic, and socio-economic factors (Rekik et al., 2025). From a technical and economic perspective, several factors influence the site selection, such as the wind speed and consistency of the site, as well as the construction costs. In terms of socio-economic implications, local residential areas can be affected by potential noise pollution and adverse visual effects on the landscape. Overall, these factors increase the complexity of determining the optimal placement. Various methodologies have been developed for determining wind farm locations, e.g., for maximizing investor profits (Huang, 2007), optimizing for grid constraints, such as voltage loss (Borges & Falcão, 2006), and methods for optimizing for both economic and environmental objectives (e.g. Cranmer et al., 2018; Cetinay et al., 2017). Similarly to the radar placement problem, evolutionary algorithms, MILP, and particle swarm optimization are typically used for wind farm placement optimization (see, e.g., Cranmer et al., 2018; Abdelsalam and El-Shorbagy, 2018; Brigada and Ryvkina, 2021).

As the placement of radars or wind farms is a complex issue in itself, the joint placement of both of these increases the complexity even further. As discussed in Section 2.3, the adverse effects of wind farms on radars are location-dependent. Therefore, optimizing the placement of radars and wind farms simultaneously can provide better results than optimizing the placements individually. However, as the number of placement options for radars and wind farms increases, the number of

placement combinations grows combinatorially, i.e., the complexity grows rapidly.

Due to the complexity of joint placement, and because air surveillance is prioritized over wind farm development, wind farms are typically sited around existing radar placements (see, e.g., Brigada and Ryvkina, 2021). The impact of a proposed wind farm on air surveillance quality is assess by the air surveillance authorities, who evaluate the suitability of the site (Joensuu et al., 2021). The simplest siting technique would be to place the wind farms such that they are outside the LOS of the radar system. However, this technique is typically not feasible as the wind farm siting options are within the air surveillance area of interest. Therefore, more refined methods are required to evaluate both the adverse effects and the joint placement of radars and wind farms.

In Lahti (2022), an approach to identifying and assessing adverse effects on air surveillance systems was developed in order to compare different radar and wind farm site options. However, this approach requires evaluating the performance of all possible placement combinations using computationally intensive simulations, which becomes infeasible with an increasing number of placement options. Hagnäs (2025) expands on this approach by developing an algorithm for optimizing the radar and wind farm placements without exhaustive evaluation of all placement combinations. However, this approach still requires complex simulations for the radar performance evaluation, which is computationally demanding and limits the number of possible placement options for radars and wind farms.

While methods, such as Lahti (2022) and Hagnäs (2025), exist for the joint optimization of radars and wind farm placements, no studies exist in the literature that address this joint optimization when a large number of placement options is considered. In order to optimize the placements, the placement problem needs to be formulated into an optimization problem, with an objective function, decision variables, and constraints. Based on the approaches used for siting radars and wind farms separately, their joint placement can be described with integer programming, where the selection of radar and wind farm sites are binary decision variables. The objective function is to maximize the air surveillance quality. The existing methods use simulations to determine the adverse effects of wind farms and the air surveillance quality. However, simulations are computationally heavy, meaning this approach becomes infeasible when a large number of placement options is considered. Therefore, approximate models are required for the radar performance, wind farm adverse effects, and the air surveillance quality. Based on the problem structure of the integer programming formulation, it can be solved using metaheuristic methods or an exact algorithm.

The benefit of using metaheuristic methods is that they impose few requirements on how the objective function and constraints in the placement problem are formulated. In particular, properties such as linearity, differentiability or convexity with regard to the decision variables are not necessary (Bandaru & Deb, 2016). Typically, algorithms such as evolutionary algorithms or particle swarm optimization may be used, as they can efficiently explore large solution spaces and handle multiple criteria. However, resulting solutions have no guarantee of being optimal (Blum & Roli, 2003). In addition, these solutions can vary every time the algorithm is executed due to its stochastic nature. This stochasticity also causes a lack of transparency in the exploration

of the solution space, which can make understanding and prediction of the algorithm's behavior difficult.

To guarantee that the radar and wind farm placements are globally optimal, the placement problem needs to be solved with an exact algorithm. However, using an exact algorithm poses limitations on the problem formulation. Exact algorithms are computationally more demanding than metaheuristic methods. Therefore, the placement problem needs to be formulated such that it can be solved with an exact algorithm even when the problem size grows. As non-linear optimization problems are generally more complex than linear problems (Hochbaum, 2007), linear formulations of the placement problem are likely to remain feasible as the problem scale increases. Therefore, in this thesis, the placement problem is formulated as a MILP problem, where the objective function and constraints are linear with regards to the decision variables. This MILP model, including the decision variables, constraints, and the objective function, is introduced in the following Section 3. This model can then be solved using existing mathematical programming solvers, which have specifically been developed for solving these types of large-scale MILP problems efficiently. This approach is more restrictive compared to the metaheuristic methods, as the objective function and constraints must be linear with regard to the decision variables. However, it offers reproducibility, guarantees of optimality, and enables a clear understanding of the factors affecting the optimal solution.

3 Optimization of radar and wind farm placement

This section considers the joint placement optimization of radars and wind farms with the objective of enabling wind energy development while maintaining high air surveillance capability. To address this optimization task, performance models are developed both for radars and the adverse effects of wind farms in Section 3.1. These models are used to evaluate the resulting air surveillance quality produced by a combination of radars and wind farms. The evaluation is conducted with performance measures presented in Section 3.2. Using these measures, mixed-integer linear programming (MILP) problems are formulated to determine the optimal placement of radars and wind farms in Section 3.3. These optimal placements are selected from a large set of feasible radar and wind farm placement options, which are provided by the respective planners. The identification of viable placement options is outside the scope of this thesis. All the placement options for wind farms are assumed to be reasonable. Therefore, evaluating and comparing the suitability of wind farm placement sites is not explicitly required for determining the placements. Thus, the only objective is to identify radar and wind farm placements, which result in high air surveillance quality.

3.1 Performance models

In the following, radar performance modeling assumptions, as well as the construction and parameterization of the wind farm adverse effect model, are based solely on an understanding of the physical principles and phenomena underlying the systems' operation, together with expert opinions from radar technology specialists. The validation of these models using data produced by more detailed sensor models or data obtained from real-world surveillance systems is beyond the scope of this thesis.

3.1.1 Radar model

In this thesis, the radar performance at a 3D location in the airspace is assumed to depend solely on the planar distance to the radar. This metric, referred to as the radar performance measure (RaPM), is a unitless value normalized between 0 and 1, where 0 represents the lowest possible performance and 1 the best possible radar performance. RaPM metric is 1 when the distance to the radar is 0 and then decreases linearly with increasing distance. The maximum distance at which a radar can see is determined by its range R. The RaPM is parametrized such that the linear decrease reaches a value of 0 at 1.5 times the maximum range of the radar. This parametrization reflects the real-life radar behavior, where the radar's performance decreases with distance and retains some capability even beyond the radar range. In reality, the range of a radar is dependent on multiple factors, such as a target's RCS and atmospheric conditions, as explained in Section 2.1. However, using a static range value is deemed sufficient for this thesis. While alternative performance models could be considered, the linear model offers a straightforward performance approximation. RaPM is visualized in Figure 1, which illustrates the gradual decrease of the performance while preserving meaningful capability within the range and limited capability beyond the range.

The radar performance is only dependent on the planar distance to the radar, i.e., vertical distance does not affect the performance. This choice is justified due to amplification of radar signals, which compensates for the increased distance and resulting radar degradation (Chen, 2004). In addition to the signal amplification, typical radars have a limited vertical coverage and cannot detect objects directly above the radar. This behavior arises from the design and orientation of the radar antenna, which is optimized to provide maximal detection range towards the horizon. However, this additional vertical effect is considered to be minor and is not taken into account by the RaPM model.

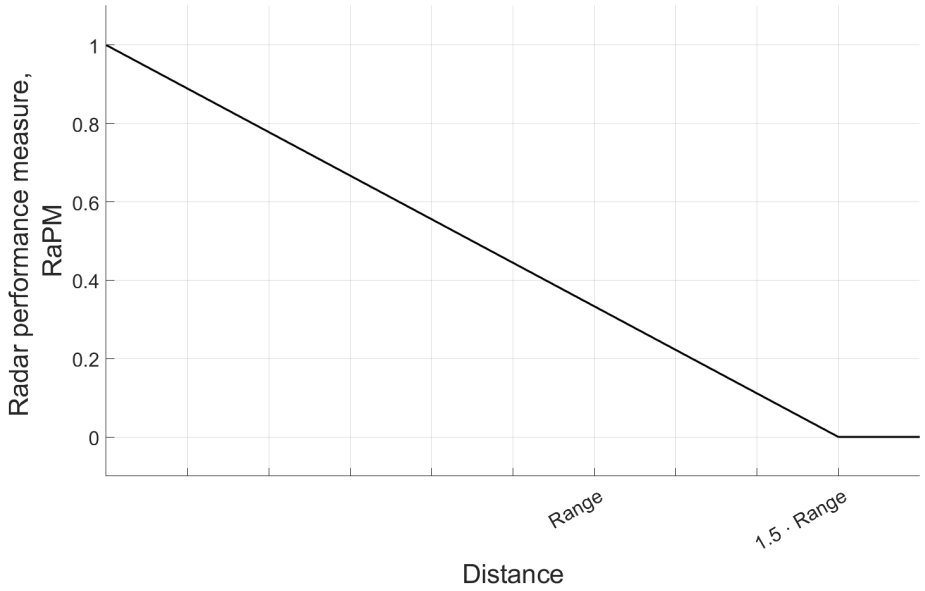

Figure 1: Radar performance measure as a function of planar distance from the radar.

The combined performance of multiple radars is calculated as the sum of all the individual radars' performance values at the evaluation location. The combined performance values are also constrained to be in $[0, 1]$, even if the computed performance values exceed 1.

3.1.2 Wind farm effect model

As discussed in Section 2.3, wind farms cause adverse effects on radar performance. To evaluate the impact of different radar-wind farm placements, an adverse effect model is first constructed. The main adverse effects considered in this thesis are the clutter effect and the shadowing effect.

The clutter effect is caused by the radar signal being scattered by the wind farm and reflected back to the radar, creating false targets and unwanted clutter in the radar image (Theil et al., 2010). This effect is localized in an area close to the wind farm, referred to as the clutter area. The clutter decreases the overall performance of the radar by increasing the false alarm rate and decreasing target detection sensitivity. Additionally, the false alarms may hinder the formation and maintenance of the target

track. The wind farm is represented as a vertical wall to describe its physical size, with height h_f and width w_f, and orientation. To describe the clutter effect, a separate vertical surface called the clutter wall is used. The clutter wall is a straight vertical plane with width w_c and height h_c. This clutter wall shares the same width and orientation as the wind farm wall, but its height can differ. The clutter area is defined as the region where a radar's LOS intersects the clutter wall and is a short distance away from the wall. Here, this distance is assumed to be 30 km, measured along the LOS. This clutter area is visualized in Figure 2 as the red dotted region.

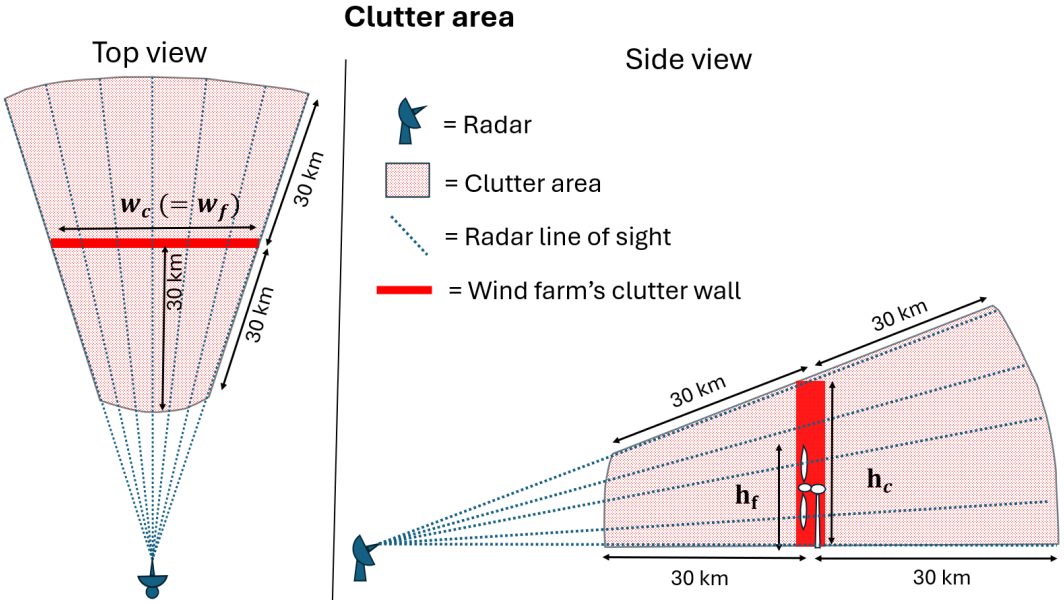

Figure 2: Top and side view of the clutter area caused by the wind farm. The red dotted area represents the region where clutter effects degrade the radar's performance. The symbols h_f and h_c represent the heights of the wind farm and the clutter wall, respectively, and w_c represents the width of the clutter wall, which is equal to the width of the wind farm w_f. The image is not to scale.

The shadowing effect is caused by the wind farm's physical obstruction of the radar beam (Leijnse et al., 2022). Therefore, the shadowing effect can be observed behind the wind farm from the radar's perspective. Similarly to the clutter effect, the shadowing effect is described by introducing a vertical surface called the shadowing wall. Its width is denoted by w_s and the height by h_s. The shadowing wall shares the same orientation and width as the wind farm wall, but the height can differ. The shadowing area is the region behind the wind farm where the radar's line of sight passes through the shadowing wall, and continues until the radar range R is reached. The shadowing area is visualized with red dots in the Figure 3, which shows the area's top and side views.

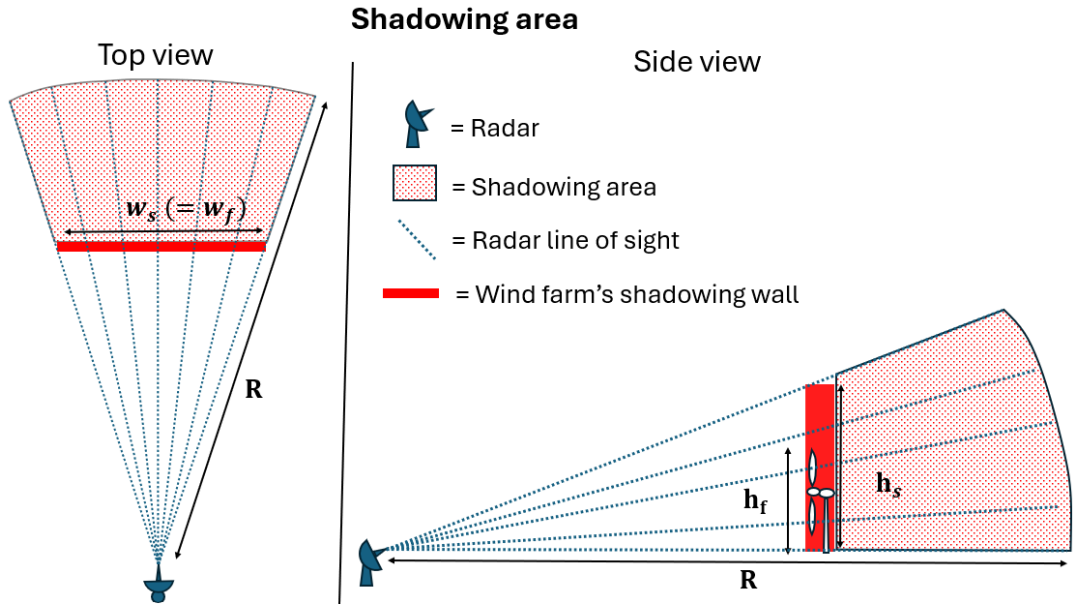

Figure 3: Top and side view of the shadowing area caused by the wind farm, where the performance of the radar is degraded due to the shadowing effect. The symbol R is used for radar range, w_s for the width of the shadowing wall, w_f for the width of the wind farm, and h_f and h_s for the heights of the wind farm and the shadowing wall, respectively. The image is not to scale.

The wind farm's location is defined in the geographic coordinate system (GCS) with coordinates (X_f, Y_f) for latitude and longitude. The terrain elevation of point (X_f, Y_f) is denoted with Z_f and is in units of meters above mean sea level. For both the clutter and the shadowing wall, the wind farm's location (X_f, Y_f, Z_f) defines the center point for the wall width and the base for the wall height. The walls are perfectly vertical, rising straight upwards from the terrain. The orientation in the horizontal plane is defined to be perpendicular to the radar's LOS toward the wind farm's position, meaning the walls are facing the radar. The orientation of the walls is determined separately for every radar. This orientation represents the worst-case scenario where, for every radar, the radar beam crosses through the maximum cross-sectional area of the turbines. Analyzing the worst-case orientations yields a conservative estimate for the clutter and the shadowing areas, capturing the full potential impact of the wind farm. This approach is further supported by the fact that the orientation of individual wind turbines can change depending on the direction of the wind (Kim & Dalhoff, 2014).

The degradation of radar performance due to the adverse effects is measured with a damping factor α_{total}. This factor indicates the percentage of how much RaPM is reduced by the wind farm. The damping factor is dependent on the magnitudes of the clutter and shadowing effects.

The magnitude of the clutter effect is expressed with a clutter factor α_c and is dependent on the distance to the wind farm. The distances are measured along the radar's LOS from where the line intersects the clutter wall. The clutter factor has

values in $[0.3, 0.5]$, where the highest factor value is at the intersection point, and the value decreases linearly with regard to the distance to the clutter wall, denoted by d_c. Therefore, the clutter factor is calculated as

$$\alpha_c = \begin{cases} 0, & \text{if } d_c > 30 \text{ km} \\ 0.5 - \dfrac{d_c}{150 \text{ km}}, & \text{if } d_c \leq 30 \text{ km} \end{cases}. \tag{1}$$

Similarly, the reduction of radar performance due to the shadowing effect is estimated with a shadowing factor α_s. The shadowing factor is dependent on the height h_{LOS} at which the radar's LOS intersects the shadowing wall, measured from the base. When the LOS intersects the wind farm at its base, the radar signal experiences more obstruction than when it intersects at the turbine tips. Thus, the shadowing factor is of the form

$$\alpha_s = \begin{cases} 0, & \text{if } h_{LOS} > h_s \\ 0.3 \cdot (1 - \frac{h_{LOS}}{h_s}), & \text{if } h_{LOS} \leq h_s \end{cases}, \tag{2}$$

where h_s is the height of the shadowing wall.

In the area closely behind the radar, the radar performance is reduced by both the shadowing and clutter effects. Assuming the reductions are independent of each other, they are combined as

$$\alpha_{total} = 1 - (1 - \alpha_c)(1 - \alpha_s). \tag{3}$$

Given that the clutter factor $\alpha_c \in [0.3, 0.5]$ and the shadowing factor $\alpha_s \in [0, 0.3]$, the resulting damping factor α_{total} is in the range $[0, 0.65]$. This range means the adverse effects can reduce the radar performance by up to 65%.

3.2 Performance evaluation

To evaluate the radar performance within the area of interest, the area is discretized into a grid with G_x horizontal and G_y vertical grid cells. Each grid cell represents a distinct geographical region of size $S_x \times S_y$, where S_x and S_y represent the size of the grid cell in x and y directions, respectively, in units of kilometers. The center of each grid cell is referred to as a grid point. These grid points are used as measurement points where RaPM and α_{total} are evaluated. This grid is applied at every examination altitude h, where $h \in H$, and H is the set of chosen examination altitudes.

The discretization allows the structured assessment of a radar's performance while maintaining computational efficiency. The grid resolution is chosen to balance accuracy and computational cost. A finer grid provides a more detailed representation of the performance, but increases the computational complexity.

The performance of individual radars and resulting radar formation is evaluated at every measurement point i, where $i \in \{1, ..., I\}$ and I is the total number of measurement points. This number is determined by the number of grid cells and the number of examination altitudes, as $I = G_x \cdot G_y \cdot |H|$. Each measurement point

i can also be presented in grid coordinates as (g_x^i, g_y^i, g_h^i), where $g_x^i \in \{1, ..., G_x\}$, $g_y^i \in \{1, ..., G_y\}$, and $g_h^i \in \{1, ..., |H|\}$.

3.2.1 Radar performance

For each radar placement $m \in \{1, ..., M\}$, where M is the number of possible radar positions, the performance of a radar located at m is calculated in all measurement points i. The performance in point i is computed by using the performance model presented in Section 3.1.1. In this model, the performance depends only on the planar distance between the measurement point and the radar. To determine these distances, the radar position m is first transformed from the GSC format into the grid coordinate system. The GCS coordinates (X_m, Y_m) for latitude and longitude, respectively, are mapped into (x_m, y_m), where $x_m \in [1, G_x]$ and $y_m \in [1, G_y]$, meaning the radar position is somewhere between the discrete measurement points (g_x^i, g_y^i). The altitude of the radar's position and the measurement points can be ignored in the performance evaluation as only the planar distance is considered.

The real-world distance between the radar and a measurement point $i = (g_x^i, g_y^i, g_h^i)$ is

$$D(m,i) = \sqrt{(g_x^i - x_m)^2 \cdot S_x^2 + (g_y^i - y_m)^2 \cdot S_y^2}, \tag{4}$$

which is used to calculate the raw radar performance metric. This measure is referred to as a raw RaPM as it does not take into account the terrain and other obstructions in the radar's LOS. This measure is calculated as

$$\text{RaPM}^{raw}(m,i) = \begin{cases} \frac{-1}{1.5 \cdot R} \cdot D(m,i) + 1, & \text{if } D(m,i) \leq 1.5 \cdot R \\ 0, & \text{otherwise} \end{cases}, \tag{5}$$

where R is the radar range in kilometers. For RaPM, the obstructions in the LOS are taken into account with a binary terrain mask $T(m,i)$, which is determined for every radar location m at every measurement point i. The $T(m,i)$ value is 1 if a radar at position m is able to see point i, and 0 if the LOS is obstructed and point i cannot be seen. RaPM is then computed as the product of the terrain mask and the raw RaPM value, i.e.,

$$\text{RaPM}(m,i) = T(m,i) \cdot \text{RaPM}^{raw}(m,i). \tag{6}$$

An example of this calculation is shown in Figure 4, where RaPM values are evaluated at some altitude h. The subplot for RaPM^{raw} shows a linear decline in performance values with distance. The terrain mask expresses which measurement points at altitude h the radar can see. The terrain mask is applied at every point as presented in Equation 6, yielding the RaPM values.

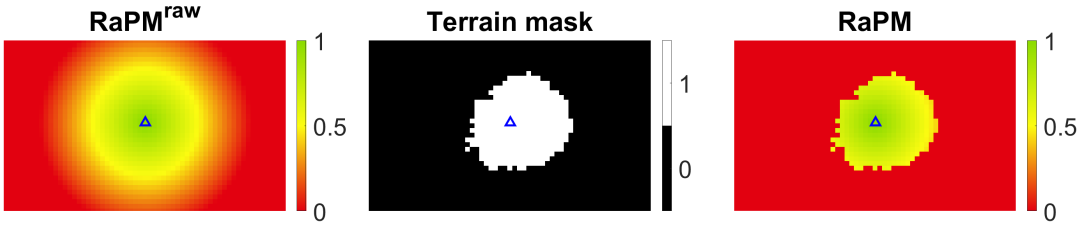

Figure 4: Illustration of RaPM before and after the terrain mask has been taken into account at some examination altitude h. The radar location is marked with a blue triangle. The left-most image visualizes the raw RaPM values, i.e., the performance of the radar if its LOS is not obstructed. The middle image visualizes the binary terrain mask, which indicates where the radar can see. The right-most image shows the RaPM values of the radar, which is the aggregation of the raw RaPM values and the terrain mask.

3.2.2 Wind farm effect

A finite set of possible wind farm locations is considered, indexed by $l \in \{1, ..., L\}$, where L denotes the number of wind farm placement options. For every radar placement option m, the subset of wind farm positions within the range R is identified. This subset contains the wind farm locations l that can cause adverse effects on the radar at the position m. Each of these radar-wind farm combinations defines an adverse effect pair (m_k, l_k). These combinations are indexed by $k \in \{1, ..., K\}$, where K is the total number of the adverse effect pairs.

The adverse effects caused by the wind farm are estimated with the damping factor α_{total}. This factor is calculated for every pair k and at every measurement point i as described in Section 3.1.2. At measurement point i, the reduction in the RaPM value for the radar at position m_k due to the wind farm at position l_k is computed as

$$A_{3D}[k, i] = \alpha_{total}(k, i) \cdot \text{RaPM}(m_k, i). \tag{7}$$

Here, A_{3D} is the 3D-adverse effect matrix, which contains possible adverse effect values. These values are computed into a matrix in order to efficiently evaluate the adverse effects between different adverse effect pairs. The size of the 3D-adverse effect matrix is $K \times I$. For increased memory efficiency, A_{3D} is stored as a sparse matrix, meaning only elements with nonzero values require memory (Gilbert et al., 1992). The use of sparse matrices is additionally reasonable, as the adverse effects are only localized near the wind farm, meaning most of the adverse effect values are zero.

3.2.3 Spatial and altitude weighting

In air surveillance, certain geographical locations may require higher surveillance quality than others due to factors such as strategic significance or population density. Similarly, some altitudes may have higher importance, which can reflect the flying altitudes of different targets. For example, drones and helicopters typically fly at low altitudes, and fighter jets at high altitudes. These importance differences in spatial

areas and altitudes are described with weights that are used in the evaluation of the air surveillance quality.

The horizontal area of interest is divided into N_A non-overlapping 2D regions, each assigned a priority reflecting its relative importance for achieving high air surveillance quality. These priorities are used to determine spatial weights w_{xy}. The weight $w_{xy}(a)$ for an area $a \in \{1, ..., N_A\}$ is computed with the centroid-weighting method (see, e.g., Ahn, 2011). In this method, the priorities are first sorted in ascending order, resulting in an importance rank q for each region. Then, the weight of the area a with importance rank q is calculated with

$$w_{xy}(a) = \frac{1}{N_A} \sum_{t=q}^{N_A} \frac{1}{t}. \tag{8}$$

In cases where multiple areas have the same priority, the weights of these areas are normalized with their average value. This normalization ensures that all areas with the same priority receive the same weight, areas with higher priority receive higher weights, and the sum of all weights equals one. To assign a spatial weight for measurement points, the weight of each area is evenly divided among all the measurement points located within that area. This ensures that the spatial weights assigned to the measurement points sum to one.

Similarly, priorities are defined for a set of altitude ranges. These altitude priorities can differ for each spatial area a. The altitude weight for an altitude range δh in area a is denoted by $w_z(a, \delta h)$, which is computed similarly to the spatial weights w_{xy}, and has the same properties. Similarly to the spatial weights, the weight of an altitude range is evenly divided among the examination altitudes belonging to that range. Thereby, the sum of altitude weights across all the examination altitudes sums to one.

3.2.4 3D-system performance measure

Here, a system refers to a specific subset of radar and wind farms chosen from the set of all possible placement options. A placement is considered selected if it is included in this system. To evaluate the air surveillance quality of such a system at different 3D-locations, a performance measure that takes into account the radar performance and wind farm adverse effects is needed. For this purpose, the 3D-system performance measure is developed. This measure is determined by aggregating the performances of the radars, as described in Section 3.1.1, and subtracting the adverse effects of the wind farms, described in Section 3.2.2. The resulting 3D-system performance measure enables comparison of systems consisting of different radar and wind farm placements.

For efficient comparison between different radar placements, the radar performances are precomputed in every 3D-measurement point into a matrix for all the placement options. The RaPM values at i for different radar placements m are stored in the performance matrix P_{3D}

$$P_{3D}[m, i] = \text{RaPM}(m, i). \tag{9}$$

In the resulting performance matrix P_{3D}, the rows correspond to the radar placement m and the columns to the measurement point. Therefore, the size of the matrix is $M \times I$. P_{3D} is stored as a sparse matrix in order to increase the memory efficiency.

The radar placement is described as a binary decision whether a placement option is selected or not. Therefore, the selection of a radar placement site in the system is represented by an indicator function

$$r_m = \begin{cases} 1, & \text{if radar location } m \text{ is selected,} \\ 0, & \text{otherwise.} \end{cases} . \tag{10}$$

Similarly, the selection of a wind farm placement site in the system is represented with an indicator function f_l

$$f_l = \begin{cases} 1, & \text{if wind farm location } l \text{ is selected,} \\ 0, & \text{otherwise.} \end{cases} . \tag{11}$$

To calculate the adverse effects of the selected wind farms on the radars, an indicator function z_k is constructed to denote which adverse effect pairs exist in the system. The function is of the form

$$z_k = r_{m_k} \cdot f_{l_k}, \tag{12}$$

where m_k and l_k are the radar and wind farm associated with the kth adverse effect pair. The indicator function z_k is active – that is, it takes the value 1 – if both the corresponding radar and wind farm are selected in the system; otherwise, it is 0. The use of indicator functions to represent the selected radar placements and the active adverse effect pairs is useful here, as the inclusion of radar performances and wind farm adverse effects in the 3D-system performance measure can be carried out with multiplication.

The 3D-system performance measure at measurement point i is obtained by summing RaPM of selected radars and subtracting the adverse effects caused by the selected wind farms. However, the resulting value of this calculation may exceed the valid range for performance measures of $[0, 1]$, explained in Section 3.1.1. As the value is not constrained, when multiple radars provide high performance values in a measurement point, the sum exceeds 1. This unconstrained performance measure is referred to as a raw 3D-system performance measure. The raw 3D-system performance measure s^{raw} is

$$s_i^{raw} = \sum_{m=1}^{M} P_{3D}[m, i] \cdot r_m - \sum_{k=1}^{K} A_{3D}[k, i] \cdot z_k. \tag{13}$$

This raw measure is used to calculate the 3D-system performance measure by constraining the values to within the valid interval of $[0, 1]$. This formula is of the form

$$s_i = \min(1, \max(0, s_i^{raw})). \tag{14}$$

To evaluate the air surveillance quality across an area of interest, the importance of different spatial areas and altitudes must be considered. The relative importance of these areas and altitude ranges is described by their weights. The spatial and altitude weights are determined as explained in Section 3.2.3. These weights are aggregated to assign a weight for an individual measurement point. The total weight of a measurement point i is

$$w_i = \frac{w_{xy}(a_i)}{I_{a_i}} \cdot \frac{w_z(a_i, \delta h_i)}{|H_{\delta h_i}|}, \tag{15}$$

where $w_{xy}(a_i)$ denotes the spatial weight assigned to the area a_i containing the measurement point i, and $w_z(a_i, \delta h_i)$ denotes the weight corresponding to the altitude range δh_i of point i within the same area. The spatial weight is divided by the number of measurement points within an area, denoted by I_{a_i}. The weight of an altitude range is divided by the number of examination altitudes within that range, denoted by $|H_{\delta h_i}|$. The total air surveillance quality of the whole area of interest is calculated as the weighted sum of weights w_i, presented in Equation 15, and the 3D-system performance measure, presented in Equation 14.

3.2.5 2D-system performance measure

The system performance measures are used as a basis for optimization formulations of the placement problem. Optimizing the placements while considering the performance in every possible 3D-measurement point is complex. If the number of 3D-measurement points is high, the placement optimization can become infeasible, meaning it cannot be solved with the available computational resources in a feasible amount of time. The optimization formulations and their complexity are discussed more in Section 3.3. In addition to computational complexity, the performance and adverse effect values are precomputed and stored in memory. With a large number of examination altitudes, the required memory can exceed the available capacity. The 2D-system performance measure is constructed to address these issues. This measure uses altitude-wise aggregated values for evaluating the performance of the selected radars and wind farms in the system, which allows the evaluation of the air surveillance quality even when the 3D-system performance measure cannot be used.

The 2D-measurement points are indexed by $j \in \{1, ..., J\}$, which corresponds to a specific horizontal grid coordinate (g_x^j, g_y^j). For each point j, a set $\mathcal{J}(j)$ is defined, such that the set includes all the 3D-measurement point indices i that share the same (g_x, g_y) coordinates but vary across the altitude levels H. Formally, this set is

$$\mathcal{J}(j) = \{i \in \{1, ..., I\} | (g_x^i, g_y^i) = (g_x^j, g_y^j)\}, \tag{16}$$

where (g_x^i, g_y^i) refers to the x- and y-grid coordinates of 3D-measurement point i, and (g_x^j, g_y^j) refers to the grid coordinates of point j. In total, the number of 2D-measurement points is $J = G_x \cdot G_y$.

The radar performance values are stored in a 2D-radar performance matrix P_{2D}. These values are obtained by aggregating the RaPM values in the 3D-measurement

points altitude-wise. To account for the varying importance of different altitudes in different spatial areas, the altitude weights w_z are used in the aggregation. Thus, the 2D-radar performance matrix values are calculated as the altitude weighted sum of the RaPM values, i.e.,

$$P_{2D}[m, j] = \sum_{i \in \mathcal{J}(j)} \frac{w_z(a_i, \delta h_i)}{|H_{\delta h_i}|} \cdot \text{RaPM}(m, i), \tag{17}$$

where $w_z(a_i, \delta h_i)$ is the altitude weight interval δh_i to which i belongs. This weight is divided by the number of examination altitudes within this altitude interval $|H_{\delta h_i}|$. Similar to the 3D-performance matrix, P_{2D} is also stored as a sparse matrix for increased memory efficiency.

The adverse effect values from wind farm interference are stored in a 2D-adverse effect matrix A_{2D}. These values are computed in a similar manner to A_{3D} defined in Equation 7, but are aggregated altitude-wise with the corresponding weights, i.e.,

$$A_{2D}[k, j] = \sum_{i \in \mathcal{J}(j)} \frac{w_z(a_i, \delta h_i)}{|H_{\delta h_i}|} \cdot \alpha_{total}(k, i) \cdot \text{RaPM}(m_k, i). \tag{18}$$

The 2D-system performance measure is obtained by adding the radar performances and subtracting the adverse effects of wind farms. Similarly to the 3D-version, these values can exceed the valid interval of $[0, 1]$. Therefore, these values are referred to as the raw 2D-system performance measure. This value is obtained with

$$s_j^{raw} = \sum_{m=1}^{M} P_{2D}[m, j] \cdot r_m - \sum_{k=1}^{K} A_{2D}[k, j] \cdot z_k. \tag{19}$$

The 2D-system performance measure value is obtained by constraining the raw values to the valid interval, i.e.,

$$s_j = \min(1, \max(0, s_j^{raw})). \tag{20}$$

Similarly to the 3D-system performance measure, the air surveillance quality for the whole area of interest is estimated by the weighted sum of the 2D-system performance measure values. The altitude weights are already included in the 2D-system performance measure when computing the radar performance and adverse effect matrices in Equations 17 and 18. Thus, the weight of measurement point j is determined only by its spatial weight, i.e.,

$$w_j = \frac{w_{xy}(a_j)}{J_{a_j}}, \tag{21}$$

where $w_{xy}(a_j)$ is the spatial weight of the area containing j, and J_{a_j} is the number of 2D-measurement points within area a_j.

3.3 Optimization formulations

The overall objective of this thesis is to introduce a way to identify radar and wind farm placements such that the resulting air surveillance quality is maximized. This placement problem is formulated as an optimization problem, where the placements of radars and wind farms are used as decision variables, and the objective is to maximize the total air surveillance quality. A MILP formulation is selected for its ability to tackle binary decision-making within a linear optimization framework (see, e.g., Vanderbei, 2020). This approach remains effective even as the problem size increases, e.g., through more decision variables or constraints, due to the efficiency of modern MILP solvers (Koch et al., 2022). It provides an efficient and scalable solution procedure, balancing model complexity and computational feasibility. The MILP formulation is constructed separately for the 3D- and 2D-system performance measures presented in Sections 3.2.4 and 3.2.5, respectively.

Since MILP relies on linear programming principles, both the objective function and the constraints must be linear with respect to the decision variables. Therefore, nonlinear expressions are converted into linear ones. The indicator functions r_m and f_l, presented in Equations 10 and 11, fit within the MILP formulation as is. However, the indicator function for the active adverse effect pairs z_k in Equation 12 is nonlinear. This function is linearized as

$$z_k \leq r_{m_k}, \forall k \in \{1, ..., K\}, \tag{22}$$
$$z_k \leq f_{l_k}, \forall k \in \{1, ..., K\}, \tag{23}$$
$$z_k \geq r_{m_k} + f_{l_k} - 1, \forall k \in \{1, ..., K\}, \tag{24}$$

where z_k is limited to $\{0, 1\}$. This linear formulation of z_k behaves the same way as in the previous product-based formulation, i.e., z_k is 1 if r_{m_k} and f_{l_k} are 1, and otherwise it is 0.

The 3D- (Equation 14) and 2D- (Equation 20) system performance measures are also nonlinear with regard to the decision variables r_m and z_k, as the raw system performance measures are clipped to be within the set $[0, 1]$. Expression 14 is linearized by setting s_i as a decision variable. The nonlinear clipping is replaced by limiting the decision variable value to be in $[0, 1]$, and setting the raw measure as an upper bound $s_i \leq s_i^{raw}$. As the objective is to maximize the sum of the s_i values, this decision variable will be appointed the maximum value it can have, i.e., s_i is either s_i^{raw} or 1. Therefore, setting s_i as a decision variable with the listed constraints behaves the same as clipping the raw value. Equation 20 for s_j is linearized in a similar manner.

As there are two alternative system performance measures, 2D and 3D, two alternative formulations for the optimization are presented. The 3D-formulation is presented in Section 3.3.1, which is based on the 3D-system performance measure introduced in Section 3.2.4. Similarly, the 2D-formulation is presented in Section 3.3.2, which is based on the 2D-system performance measure introduced in Section 3.2.5. The differences in these formulations are discussed in more detail in Section 3.3.3

3.3.1 3D-formulation

When formulating a MILP problem, the objective function, decision variables and constraints are determined. The objective is to maximize the air surveillance quality in the whole area of interest. The air surveillance quality in a 3D-measurement point is measured by the 3D-system performance measure 14. To account for the varying importance levels of different spatial areas and altitudes, the system performance measure values are weighted with w_i, given by Equation 15. The objective is then to maximize the sum of the weighted 3D-system performance measure values.

The binary indicator functions 10 and 11 for radar and wind farm placements are implemented as binary decision variables in the optimization model. This means the selection of radars and wind farms in the system, which maximize air surveillance quality, is determined by an optimization solver. This optimization solver is a computational tool, which uses some optimization algorithm to explore feasible solutions and determine the solution, which maximizes the objective function. In addition to the radar and wind farm placements, the indicator function for adverse effect pairs z_k and the 3D-system performance measure s_i are also treated as decision variables. These variables are implemented as decision variables for linearity. However, their value is dependent on the radar and wind farm placements r_m and f_l, as the placements determine the active adverse effect pairs and the air surveillance quality. This dependency is achieved in the optimization formulation through constraints.

The active adverse effect pairs, i.e., z_k values, are dependent on which radars r_m and wind farms f_l are selected in the system. This dependency is formulated linearly by using Equations 22 - 24 as constraints. Similarly, the 3D-system performance measure s_i is dependent on the radar and wind farm placements. The s_i value is constrained to be less than or equal to the raw 3D-system performance measure, which is presented in Equation 13. Lastly, the numbers of selected radars and wind farms are set to be n_r and n_f, respectively.

Using the objective function, decision variables and constraints introduced above, the resulting 3D-formulation of the radar and wind farm placement optimization problem is

$$\max_{s,r,f,z} \sum_{i=1}^{I} w_i \cdot s_i \tag{25}$$

subject to

$$s_i \leq \sum_{m=1}^{M} P_{3D}[m,i] \cdot r_m - \sum_{k=1}^{K} A_{3D}[k,i] \cdot z_k, \forall i \in \{1,...,I\} \tag{26}$$

$$\sum_{m=1}^{M} r_m = n_r \tag{27}$$

$$\sum_{l=1}^{L} f_l = n_f \tag{28}$$

$$z_k \leq r_{m_k}, \forall k \in \{1,...,K\} \tag{29}$$

$$z_k \leq f_{l_k}, \forall k \in \{1,...,K\} \tag{30}$$

$$z_k \geq r_{m_k} + f_{l_k} - 1, \forall k \in \{1,...,K\} \tag{31}$$

$$s_i \in [0,1], \forall i \in \{1,...,I\} \tag{32}$$

$$r_m \in \{0,1\}, \forall m \in \{1,...,M\} \tag{33}$$

$$f_l \in \{0,1\}, \forall l \in \{1,...,L\} \tag{34}$$

$$z_k \in \{0,1\}, \forall k \in \{1,...,K\} \tag{35}$$

Decision variables

s_i : 3D-system performance measure value at measurement point i

r_m : Indicator function whether radar at position m is selected

f_l : Indicator function whether wind farm at position l is selected

z_k : Indicator function whether both radar r_{m_k} and wind farm f_{l_k} are selected

Auxiliary variables

i : 3D-measurement point

P_{3D} : Performance of radar m at point i

A_{3D} : Adverse effects of wind farm l_k on radar m_k at point i

w_i : Total weight of point i

Parameters

n_r : Number of radars to place

n_f : Number of wind farms to place

M : Number of radar placement options

L : Number of wind farm placement options

K : Number of possible adverse effect pairs

I : Number of 3D-measurement points

In the 3D MILP formulation, the objective function in Equation 25 is defined as the maximization of the weighted sum of the 3D-system performance measure values s_i. The s_i values are used as decision variables in Equation 32, which can have values in $[0, 1]$, but is then constrained to be less than the raw 3D-system performance measure values in Equation 26. The radar and wind farm placements are also used as decision variables in Equations 33 and 34. The numbers of radar and wind farm placements must be equal to the given parameters n_r and n_f, which is stated by Equations 27 and 28. The radar and wind farm placements selected in the system determine the active adverse effect pairs k, i.e., the values of the indicator function z_k. For linearity, the indicator function z_k is used as a decision variable in Equation 35. Then, the constraints 29 - 31 are used to restrict its value based on the selected radar and wind farm placements.

In total, the number of decision variables is $I + M + L + K$. For the number of constraints, Equation 26 defines I constraints, Equations 29-31 define K constraints each, and Equations 27 and 28 account for one constraint each. Therefore, the total number of constraints is $3K + I + 2$.

3.3.2 2D-formulation

The 2D-formulation of the radar and wind farm placement optimization problem is constructed similarly to the 3D-formulation, except that it is based on the 2D-system

performance measure presented in Section 3.2.5. The objective function of the resulting MILP problem is to maximize the sum of spatially weighted 2D-system performance measure values s_j. With the 2D-formulation, the system performance measure values are already weighted altitude-wise, thus only spatial weights w_{xy} are required.

Decision variables in the 2D-formulation are the indicator functions for radar and wind farm placements r_m and f_l, respectively. As discussed previously, the 2D-system performance measure values s_j and the indicator function for adverse effect pairs z_k are also used as decision variables.

The indicator function z_k is constrained with Equations 22 - 24 to determine its value based on radars and wind farms selected in the system. The decision variable s_j is constrained to be less or equal to the raw 2D-system performance measure, presented in Equation 19. This constraint ensures the value of the variable s_j is determined by the radars and the wind farms selected in the system. The numbers of the selected radars and wind farms are constrained to be n_r and n_f, respectively.

The 2D-formulation is of form

$$\max_{s,r,f,z} \sum_{j=1}^{J} w_j \cdot s_j \tag{36}$$

subject to

$$s_j \leq \sum_{m=1}^{M} P_{2D}[m,j] \cdot r_m - \sum_{k=1}^{K} A_{2D}[k,j] \cdot z_k, \forall j \in \{1,...,J\} \tag{37}$$

$$\sum_{m=1}^{M} r_m = n_r \tag{38}$$

$$\sum_{l=1}^{L} f_l = n_f \tag{39}$$

$$z_k \leq r_{m_k}, \forall k \in \{1,...,K\} \tag{40}$$

$$z_k \leq f_{l_k}, \forall k \in \{1,...,K\} \tag{41}$$

$$z_k \geq r_{m_k} + f_{l_k} - 1, \forall k \in \{1,...,K\} \tag{42}$$

$$s_j \in [0,1], \forall j \in \{1,...,J\} \tag{43}$$

$$r_m \in \{0,1\}, \forall m \in \{1,...,M\} \tag{44}$$

$$f_l \in \{0,1\}, \forall l \in \{1,...,L\} \tag{45}$$

$$z_k \in \{0,1\}, \forall k \in \{1,...,K\} \tag{46}$$

Decision variables

s_j : 2D-system performance measure value at measurement point j

r_m : Indicator function whether radar at position m is chosen

f_l : Indicator function whether wind farm at position l is chosen

z_k : Indicator function whether both radar r_{m_k} and wind farm f_{l_k} are chosen

Auxiliary variables

j : 2D-measurement point

P_{2D} : Performance of radar m at point j

A_{2D} : Adverse effects of wind farm l_k on radar m_k at point j

w_j : Spatial weight for point j

Parameters

n_r : Number of radars to place

n_f : Number of wind farms to place

M : Number of possible radar placement options

L : Number of possible wind farm placement options

K : Number of possible adverse effect pairs

J : Number of measurement points

The objective function, defined in Equation 36, is to maximize the weighted 2D-system performance measure values s_j. The weight w_j is defined in Equation 21, and contains only the spatial weight, as the altitude weights are already considered in the altitude-wise aggregation. The s_j values are used as decision variables in Equation 43. They are constrained by Equation 37 to be less than the raw 2D-system performance performance measure values. The raw performance value is determined by which radar and wind farm placements are selected in the system. These selections are used as decision variables in Equations 44 and 45. The total number of radars is set to be n_r in Equation 38, and total number of wind farms to be n_f in Equation 39. The radar and wind farm placements determine the active adverse effect pairs. The active adverse effect pairs k are expressed linearly by setting z_k as a decision variable, and constraining it to be dependent on the radar and wind farm placements r_m and f_l. These constraints are expressed in Equations 40 - 42.

In total, the number of decision variables is $J + M + L + K$. The constraint for s_j in Equation 37 accounts for J constraints. The number of radars and wind farms, corresponding to Equations 38 and 39, account for one constraint each. Equations 40 - 42 define the constraints for the decision variable z_k, each encompassing K individual constraints. Thus, the total amount of constraints is $3K + J + 2$.

3.3.3 Comparison of 2D- and 3D-formulations

The radar and wind farm placement optimization is formulated as a MILP problem using two formulations: 2D and 3D. These formulations differ primarily in how they represent the radar spatial performance and balance performance accuracy with computational complexity. Both formulations have strengths and weaknesses, and the appropriate choice depends on the available computational resources and the intended use of results.

The 3D-formulation offers more accurate assessment of radar performance and wind farm effects than the 2D-formulation, as the performance is evaluated at individual 3D-measurement points. However, the accuracy of the problem formulation entails a trade-off involving greater computational complexity and higher memory demands. As discussed in Section 3.3.1, the number of decision variables and constraints increases linearly with the number of measurement points $|I|$. This number influences the computational feasibility of the MILP problem, determining whether it can be solved within a reasonable time frame given the available computational resources. In addition, the size of the 3D-performance matrix P_{3D} and the 3D-adverse effect matrix A_{3D} also grow linearly with the number of measurement points I. This number increases with a larger area of interest, a greater number of examination altitudes $|H|$, or with higher spatial resolution, which defines the number of grid cells used to cover the area of interest. As I increases, the MILP problem can exceed available memory capacity or become computationally infeasible.

When the 3D-formulation becomes infeasible to solve, the problem may still be addressed using the 2D-formulation. In this formulation, the performance measure and adverse effect values are aggregated altitude-wise, and the resulting values are represented in 2D-measurement points j. Similarly to the 3D-formulation, the number of decision variables and constraints is linearly dependent on the number of 2D-measurement points J. However, as the performance values are aggregated altitude-wise, the number of 2D-measurement points is $J = \frac{I}{|H|}$, i.e., $|H|$ times less than the number of 3D-measurement points. By reducing the number of measurement points, the 2D-formulation remains computationally and memory feasible even when the 3D-formulation cannot. However, aggregating the measurement points involves a trade-off in the accuracy of optimization results. The 2D-formulation is accurate for individual radar performances, but the combined performance of multiple radars can be distorted. In the 2D-formulation, the combined performance is obtained by summing the aggregated 2D-performance measure values from each radar. This aggregation means that the radar performance is only determined by the aggregated value and not by the performances at different altitude levels. Thus, this approach can lead to a situation where at some horizontal location (x, y), the combined radar performance can have value 1, i.e., the maximum value, even though no radar provides coverage at lower altitudes. Even if the individual radar performances are poor, given enough overlapping coverage, the sum of the aggregated values can be 1. Therefore, in areas covered by multiple radars, the 2D-system performance measure values are typically higher than those obtained using the 3D-formulation. Despite these limitations, the 2D-formulation provides a good approximate solution and should be used when the

3D-formulation becomes computationally infeasible or only an approximate solution is needed.

The differences in the formulations are highlighted in Section 4 through an example problem. This section compares the formulations in terms of optimal placements, memory requirements, and the time taken by the solution of the example problem.

4 Example problem

To demonstrate the effectiveness and utility of the placement method developed in this thesis, an example problem is considered in which radars are placed across Finland, and wind farms are placed in Eastern Finland. Additionally, a large number of placement options are considered to test and demonstrate the feasible scale of the placement problem. These placement options for radars and wind farms are purely fictitious and do not reflect any actual sites or development intentions. This problem setup is motivated by the lack of wind farm development in Eastern Finland (Peiponen, 2022).

The example problem is solved with both the 3D- and 2D-formulations, presented in Sections 3.3.1 and 3.3.2, respectively. This example is used to examine the differences in the optimal radar and wind farm placements and the resulting air surveillance qualities with alternative formulations.

Additionally, spatial and altitude weights are used to take into account the relative importance of good air surveillance for different areas and altitudes. As the wind farms are placed in Eastern Finland, higher importance is given to the eastern areas for good air surveillance. To analyze the effect of the weighting, the optimal radar and wind farm placements are also calculated with uniform weights.

4.1 Problem setup

In the example, air surveillance in Finland is considered. However, the example problem is fully fictitious, and the problem setup, meaning the area of interest, the area division, weights, and the radar and wind farm placement options are fictitious and are made up only to demonstrate the developed placement method.

The objective is to place 20 radars and 60 wind farms such that the overall air surveillance quality in the whole area of interest is maximized. The area of interest is limited to approximately 300 km from the Finnish border. This region is divided into 13 areas for which spatial and altitude weights are determined. The area division is presented in Figure 5, where areas 1-9 represent Finland's inland area, and the North, East, South, and West represent the outer surrounding areas.

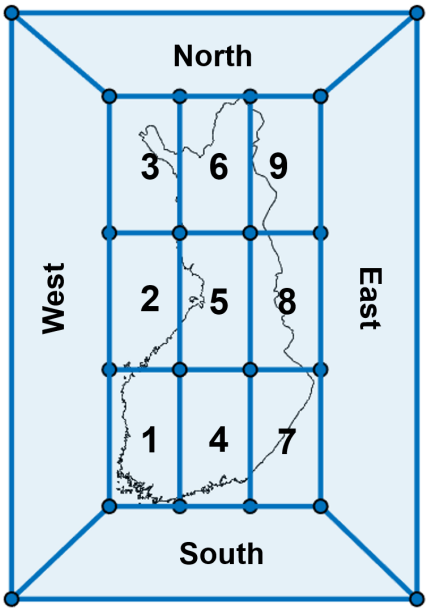

Figure 5: Division of the area of interest to which spatial and altitude weights are given.

The altitude weights are determined by the priorities of different altitude ranges. In this example, two types of altitude priority classes are considered: low-altitude priority and equal altitude priority. The low-altitude priority class gives higher priority to the lower altitude range, meaning low-altitude ranges have higher importance on good air surveillance quality than the higher altitude ranges. In the equal altitude priority class, equal priority is set for every altitude range. The examination altitudes considered are between 0 and 15 kilometers, and priorities are given for every 1-kilometer interval. The priorities for the altitude classes are given in Table 1.

Table 1: Altitude ranges and priorities.

Altitude range	Low-altitude priority class	Equal altitude priority class
(0 km, 1 km]	1	1
(1 km, 2 km]	2	1
(2 km, 3 km]	2	1
(3 km, 4 km]	2	1
(4 km, 5 km]	2	1
(5 km, 6 km]	3	1
(6 km, 7 km]	3	1
(7 km, 8 km]	3	1
(8 km, 9 km]	3	1
(9 km, 10 km]	3	1
(10 km, 11 km]	4	1
(11 km, 12 km]	4	1
(12 km, 13 km]	4	1
(13 km, 14 km]	4	1
(14 km, 15 km]	4	1

Priorities on air surveillance quality are determined for the 13 different spatial areas presented in Figure 5. As this example problem is motivated to enable wind farm development in Eastern Finland while maintaining high air surveillance quality, higher priority is given to the eastern areas. The low-altitude priority class is used for inland areas, i.e., areas 1-9. This class is chosen due to the need to be able to detect low-flying objects, such as drones. Drones have a limited range, meaning they are typically launched near targets. Therefore, their detection far outside the Finnish border is not as important as their range does not reach the border. For outer areas, i.e., North, East, South, and West, the equal altitude priority class is used due to the varying flying objects that need to be detected. For example, fighter jets and bombers fly at high altitudes, helicopters at medium altitudes, and drones at low altitudes.

Spatial priorities, resulting spatial weights, and altitude priority classes for all areas are given in Table 2. The spatial weight column presents the total weight of the spatial area, and the spatial weight per point column presents the spatial weight of a measurement point within an area. The spatial weight per point is dependent on the number of measurement points within an area, i.e., its size. As pointed out by Table 2, the area with the highest priority does not mean it has the highest weight per point. As the surrounding areas are large, they contain more measurement points than the spatial areas 1-9. Therefore, the weight of an individual measurement point is smaller but the total weight of the area is larger.

Table 2: The spatial priority, the spatial weight of the area, the spatial weight per point, and the altitude priority class for all areas are presented. The spatial weight per point is scaled with a factor 10^{-3} for clarity.

Area	Spatial priority	Spatial weight	Spatial weight per point ($\cdot 10^{-3}$)	Altitude priority class
1	6	0.0125	0.07	Low-altitude
2	6	0.0125	0.07	Low-altitude
3	6	0.0125	0.07	Low-altitude
4	4	0.0456	0.24	Low-altitude
5	4	0.0456	0.24	Low-altitude
6	5	0.0270	0.14	Low-altitude
7	2	0.1212	0.64	Low-altitude
8	2	0.1212	0.64	Low-altitude
9	2	0.1212	0.64	Low-altitude
North	3	0.0690	0.13	Equal
East	1	0.2446	0.27	Equal
South	2	0.1212	0.21	Equal
West	4	0.0456	0.05	Equal

To evaluate how the spatial and altitude weights given in Table 2 affect the optimal radar and wind farm placements, the example problem is also solved with uniform weighting. With the uniform weighting, all areas have the equal altitude priority class, which is defined for the altitude intervals presented in Table 1. The uniform altitude priorities are assigned to altitude ranges rather than individual examination altitudes in order to not overemphasize the lower altitudes. In contrast, the spatial weights are determined for the individual measurement points and not the spatial areas. This point-wise weighting ensures that every measurement point has the same spatial weight, and the size of the spatial area does not affect the weight of the measurement points it contains.

4.2 Placement options

4.2.1 Radar sites

As discussed in Section 2.1, the placement of radars affects the resulting air surveillance quality. A possible placement option should provide a radar with a clear LOS, without obstructions from the terrain. This unobstructed LOS is typically achieved by placing the radars on locally elevated terrain, such as hills. In this example, these elevated terrain locations are used as placement options for the radars.

The elevated terrain locations are found by analyzing the topographic map of Finland. A rectangle is drawn around the area of Finland to define the region where the possible radar locations are searched. To analyze the local areas more deeply, this rectangle is divided into 15 parts both vertically and horizontally, resulting in 225

smaller windows. The rectangle and the window division are presented in Figure 6. Each of the windows covers an area approximately 80×40 km^2. From each window, the five most elevated locations are selected, such that the distances between these locations are at least 10 kilometers, and higher elevation is prioritized. This constraint prevents the potential radar sites from being placed on the same hilltop. Once the potential radar sites are obtained for all the windows, the sites again filtered, such that the distance between these sites is at least 10 kilometers. This distance constraint is applied again because the elevated terrain features, i.e., hills, can get divided into multiple windows.

The windows also partly cover the neighboring countries and the sea. However, only the potential radar sites within the Finnish border are considered. Additionally, the radars are not allowed to be placed right on the border. Therefore, the remaining placement options are filtered such that only the sites that are inside Finland and more than 40 km away from the border remain.

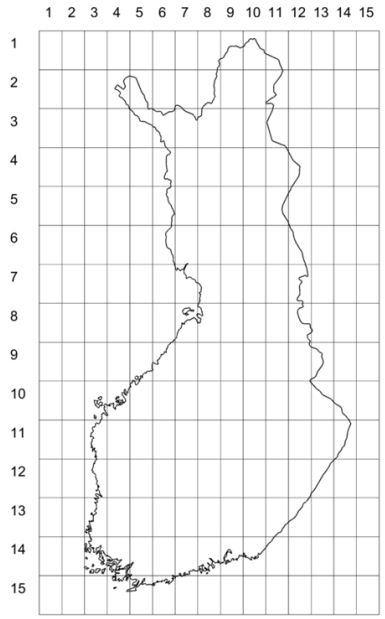

Figure 6: Grid division used for local elevated terrain search. Potential radar sites are identified by determining elevated terrain locations from each window.

With the discussed approach, 315 potential radar placement options are found, which are presented in Figure 7 in blue. The placement options are not realistic for real air defense use as this leaves out the north-west region without radar placement options. However, these locations are sufficient in demonstrating the capability of the placement method, as the number of possible air surveillance systems – i.e., the number of feasible solutions – with 20 radars is $\binom{315}{20} \approx 2 \cdot 10^{31}$.

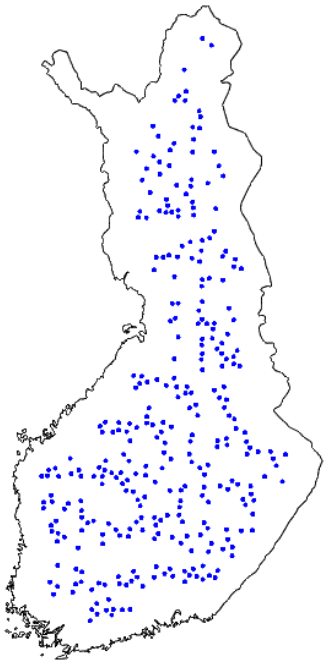

Figure 7: Possible radar placement options for 20 radars used for the example problem. The number of placement options is 315. These placement options for radars are purely fictitious and do not reflect any actual sites or plans.

4.2.2 Wind farm sites

The siting of wind farms is discussed in Section 2.4. However, finding suitable placement options for wind farms is out of scope for this thesis. Therefore, the large number of wind farm placement options is determined by randomly selecting 468 placement options from Eastern Finland. The placement options are visualized with red dots in Figure 8. Similarly to the radar placement options, some of the possible wind farm sites can be unrealistic, but these options are sufficient in demonstrating the potential number of wind farm placement options and the size of the example problem. The number of ways to choose 60 wind farms from the 468 placement options is $\binom{468}{60} \approx 4 \cdot 10^{80}$.

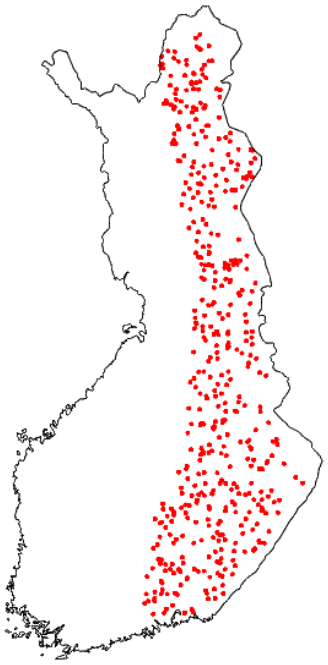

Figure 8: Possible wind farm placement options for 60 wind farms used for the example problem. The number of placement options is 468. These placement options for wind farms are purely fictitious and do not reflect any actual sites or development intentions.

As the placement options for wind farms are randomly generated, two or more sites may be located closer to each other than the size of one wind farm. To prevent this, a distance constraint is added to the placement of wind farms, such that the distance between any two wind farms must be at least 20 kilometers. This distance limit is reasonable due to the large size of the placed wind farms.

Additionally, the wind farms should be placed all over the eastern region. Therefore, an additional regional constraint is added. The placement options are divided into three location categories: North, Middle, and South. The wind farm placement options and their placement categories are visualized in Figure 9. In the figure, the placement options belonging to the category North is presented in red, Middle with yellow, and South with purple. The placement of wind farms is constrained such that 20 wind farms must be placed in each of these location categories.

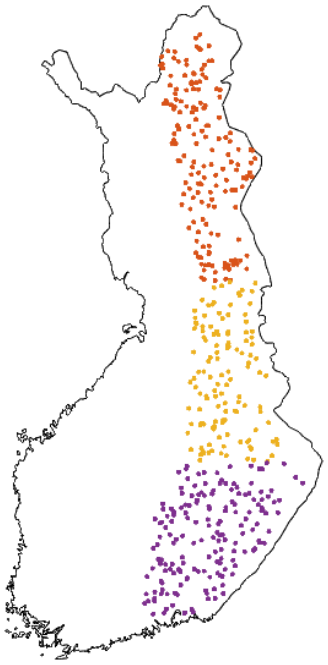

Figure 9: Location categories of the possible wind farm placement options. The North category placements are depicted with red dots, the Middle category with yellow dots, and the South category with purple dots. These placement options for wind farms are purely fictive and do not reflect any actual sites or development intentions.

4.3 Model parametrization

In this example, the number of radars to be placed is $n_r = 20$, which have a range of $R = 300$ km. The number of radar placement options is $M = 315$. The number of wind farm placement options is $L = 468$, from which $n_f = 60$ wind farms are placed. The wind farms are considered to be 5 km wide and 300 meters high. The size of the clutter wall is set to be $w_c = 5$ km wide, i.e., same as the width of the wind farm, and the height is $h_c = 600$ m, i.e., two times the height of the wind farm. The clutter wall is higher than the wind farm to account for beam width of the radar, as clutter can occur even when the wind farm does not interrupt the LOS directly. The shadowing wall is set to be $w_s = 5$ km wide, same as the wind farm, and $h_s = 450$ m high, i.e., 1.5 times the height of the wind farm. h_s is higher than the wind farm to account for the shadowing effects caused by the wind farm being within the Fresnel zone of the radar signal.

The calculations are performed with a resolution of $S_x \times S_y = 20 \times 20\,\text{km}^2$, meaning the measurement points are spaced 20 kilometers apart. The measurements are performed in a $1720 \times 2020\,\text{km}^2$ size area, corresponding $G_x = 101$ and $G_y = 86$ grid points. In computation, 19 examination altitudes are used: four below 1 km (200 m, 400 m, 600 m, and 800 m) and fifteen from 1 km to 15 km at 1 km intervals (i.e., 1 km, 2 km, ..., 15 km). As five examination altitudes are within the (0 km, 1 km] interval, the altitude weight of this interval is divided equally between these examination altitudes.

4.4 Optimal solutions

The optimal placements and the resulting system performance measures are determined with both the 2D- and 3D-formulations. The problem is solved with the non-uniform weighting, presented in Table 2, as well as with the uniform weighting. The differences in the optimal solutions calculated with the 2D- and 3D-formulations are discussed in Section 4.4.3. In addition, this section discusses the effect of the weighting to the optimal placements by comparing the optimal solutions.

The optimization is performed with Gurobi Optimizer v12.0.1 via the Matlab interface, using the dual simplex algorithm (e.g., Padberg, 2013). The computations are carried out on a laptop with AMD Ryzen 7 5800U with Radeon Graphics CPU 1.90 GHz and 16 GB RAM, running Windows 11.

4.4.1 3D-formulation

The example problem is solved with non-uniform and uniform weights with the 3D-formulation, presented in Section 3.3.1. With this formulation, there are $J = 8686$ 2D-grid points and $|H| = 19$ examination altitudes. Therefore, the number of 3D-grid points is $I = J \cdot |H| = 165034$. With the 315 radar placement options visualized in Figure 7 and 468 wind farm placement options visualized in Figure 8, there are $K = 71339$ adverse effect pairs.

In order to visualize the 3D-system performance measure values, the 3D-values are aggregated with an altitude-wise weighted sum. The aggregation is conducted for every 2D-grid point j as

$$\sum_{i \in \mathcal{J}(j)} \frac{w_z(a_i, \delta h_i)}{|H_{\delta h_i}|} \cdot s_i, \tag{47}$$

where $\mathcal{J}(j)$ is defined in Equation 16, and $w_z(a_i, \delta h_i)/|H_{\delta h_i}|$ is the weight of the examination altitude. Even though this aggregation is similar to the one performed for the 2D-formulation, the optimal solution and the aggregated s_i values will differ from the 2D-version, as the aggregation is performed after calculating the 3D-system performance values.

The optimal placement options and the resulting 3D-system performance measure obtained with the non-uniform weighting are visualized in Figure 10. The radar placements are presented with blue triangles, and the wind farm placements with black crosses. The resulting 3D-system performance measure values are aggregated altitude-wise. The aggregated values are visualized with a color gradient, where red signifies low values and green high values. Based on the figure, the radars are spread out across Finland and can be seen to be placed near the border. The radars are fairly evenly placed, meaning no large gaps can be seen in the radar placements. While the wind farms are fairly evenly distributed across the eastern region, their overall placement is more concentrated towards the center of Finland. The performance measure values can overall be considered good as almost the entire area within Finland is colored green, corresponding to values over 0.8. The performance of the radars appears to drop near the border of the inland areas, meaning areas 1-9 in Figure 5,

which is especially visible in the northwest corner. This performance drop is due to the distance to the radars and the altitude weighting. As the border of the inland area is in some parts far away from the radars, no radar coverage can be provided in the lower altitudes. This limited low altitude coverage is due to the measurement points being farther away than the radar horizon, meaning the Earth's curvature prevents the radar from covering the lower altitudes. This decreased performance at low altitudes is additionally highlighted in the performance value visualization by the higher weight set for the low altitudes. As the 3D-system performance measure values are aggregated altitude-wise for visualization, the higher weight of low altitudes causes their value to affect the aggregated value more than the higher altitude performance values. As the surrounding area has uniform altitude weighting, the lack of coverage in the lower altitudes is not highlighted. Therefore, the aggregated performance values is higher in the surrounding area. This difference in the altitude weighting causes the border of the inland areas to be visible in the aggregated results in the Figure 10. The performance measure values in the surrounding areas decrease with distance to the radars. The system performance measure values can be seen to be zero in some parts of the surrounding areas, which is due to the distance being over 450 km to the nearest radar. Overall, the optimal placement of the radars and the wind farms result in good performance measure values across the area of interest with the adverse effects of the wind farms being minimized.

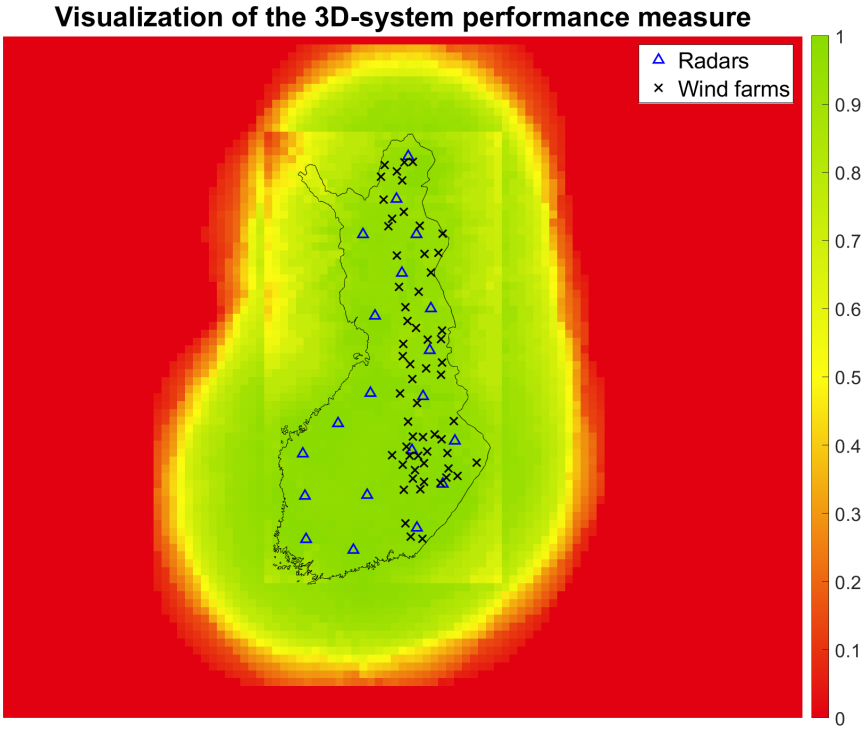

Figure 10: Optimal placement of radars and wind farms and the resulting system performance measure calculated with the non-uniformly weighted 3D-formulation. The 3D-system performance values are aggregated altitude-wise for visualization using Equation 47. The inland area, corresponding to areas 1-9, appear to have lower performance values at its borders, which is due to the different altitude weighting class used in the surrounding areas. The placements of radars and wind farms are purely fictitious and do not reflect any actual sites or development intentions.

The optimal placements and the resulting 3D-system performance measure, when uniform weighting is used, is visualized in Figure 11. Similar to using non-uniform weights, the radars are placed fairly evenly across Finland. The wind farms are also placed fairly evenly across the placement options. The resulting aggregated system performance value is good as the whole inland area as well as the surrounding areas are mostly green. In contrast to Figure 10, no boundary between the inland and the surrounding areas can be seen due to every spatial area having the same uniform altitude weighting. The 3D-system performance values within the borders of Finland can be considered very good due to the bright green color. The placed wind farms cause no visible blind spots to the radars or deficiencies in the air surveillance quality. The radar performance measure values diminish with distance, and the aggregated system performance measure values can be seen to gradually diminish farther away in the surrounding areas.

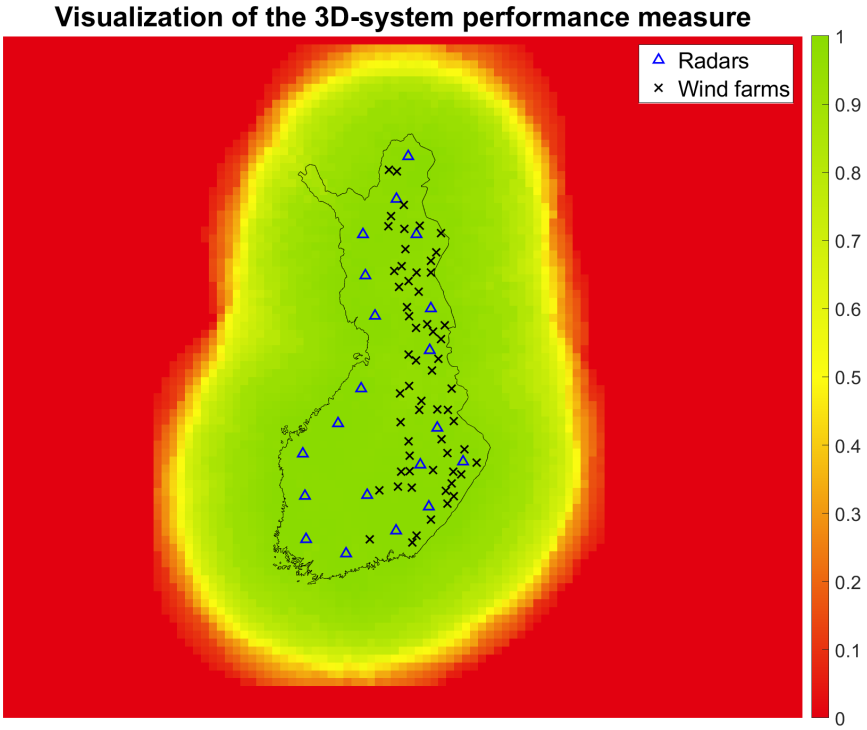

Figure 11: Optimal placement of radars and wind farms and the resulting system performance measure calculated using the 3D-formulation with the uniform weighting. The results are aggregated altitude-wise for visualization using Equation 47. The placements of radars and wind farms are purely fictitious and do not reflect any actual sites or development intentions.

Visualization of the adverse effects of the wind farms on the radars is presented in Figure 12. The values are calculated with $\sum_{k=1}^{K} A_{3D}[k,i] \cdot z_k$ for every 3D-measurement point i. Similarly to the 3D-system performance measure, the 3D-adverse effect values are aggregated altitude-wise with the altitude weights. In Figure 12, the adverse effects to the radars from the optimally placed wind farms is visualized on the left using non-uniform weighting and on the right with uniform weighting. The adverse effect values are colored for range $[0, 0.15]$ for increased clarity, even though the values belong to the range $[0, 0.65]$. In Figure 12, the adverse effect values appear to be significantly higher with the non-uniform weighting than with the uniform weighting, as can be seen from the red and orange colors. This difference is likely due to the altitude weighting used in the non-uniform weighting, where the lower altitudes have a higher weight. As discussed in Section 3.1.2, the severity of the shadowing effect is determined by the height at which the radar LOS intersects the shadowing wall. As the LOS for measurement points at low altitude is more likely to intersect the wind farm at low height, the shadowing effect is greater at lower altitudes. Therefore, the low altitudes are likely to have higher adverse effect values than the high altitudes, and the higher weight on the low altitudes highlights this difference. However, even with the non-uniform weighting, the adverse effect values are not as large as the visual suggests, as the color grading being limited to the range $[0, 0.15]$ to better present the adverse

effects. On the other hand, even with this limited color grading, the adverse effects with the uniform weights are barely visible. Minimal color differences can be seen in the right image of Figure 12, which correspond to values less than 0.1. However, even though these visualizations highlight the differences in the adverse effect values, the objective of the optimization is to maximize the 3D-system performance measure values. It is possible that a different placement of the wind farms could have produced less severe adverse effects. However, the coverage of the radars overlap in the areas with adverse effects, resulting in high 3D-system performance measure values. Therefore, although the adverse effect values appear high with the non-uniform weights, the placement of both radars and wind farms result in a good air surveillance quality in the area of interest, as pointed out in Figure 10.

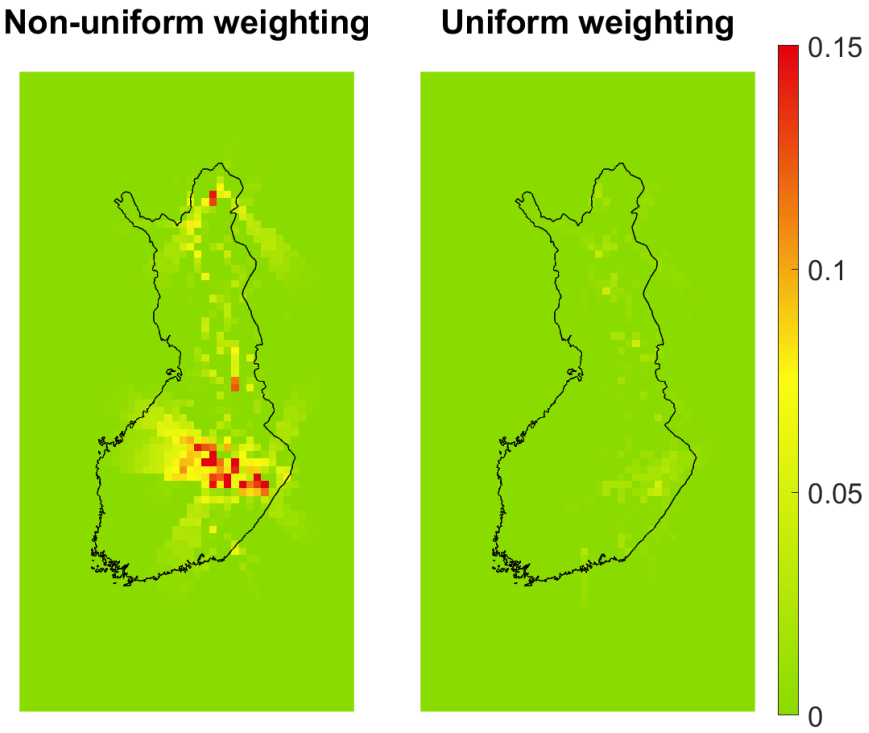

Figure 12: Visualization of the adverse effects caused by the optimally placed wind farms on the radars. The adverse effect values are aggregated altitude-wise for visualization, and the colorbar is constrained to [0, 0.15] for increased clarity.

4.4.2 2D-formulation

The optimal radar and wind farm placements are also solved with the 2D-formulation presented in Section 3.3.2, with using both the uniform and non-uniform weighting. The number of 2D-measurement points is $J = 8686$. Otherwise, the number of model variables is similar to the 3D-formulation, i.e., $M = 315$, $L = 468$, $|H| = 19$, and $K = 71339$.

As the 2D-system performance measure values are already aggregated altitude-wise, the performance values s_j can be visualized without modification. The visualizations

are similarly presented with a color gradient where red corresponds to low performance measure values and green to high values.

The optimal placement for the radars and the wind farms calculated with non-uniform weighting and with the 2D-formulation is presented in Figure 13. The radars are placed near the borders fairly evenly. The wind farms are placed across the placement options with slightly more wind farms in the center region of Finland. The resulting 2D-system performance measure values are high in the inland and surrounding areas, reaching the maximum possible value of 1 in large portions of both regions. Compared to the aggregated 3D-system performance measure values presented in Figure 10, the 2D-system performance measure values are higher. This difference is due to the effect described in Section 3.3.3, where measurement points with overlapping coverage receive a higher value with the 2D-formulation than it would with the 3D-formulation. The outline of the inland area, corresponding to areas 1-9 in Figure 5, can be detected in the 2D-values due to the higher weight given to lower altitudes. Similarly to the 3D-formulation, the northwest region of the inland area shows a poorer performance as no radars are able to cover the lower altitudes. In the surrounding area, the performance values decrease with regards to the increasing distance from the radars and reach zero when the distance is over 450 km. Overall, the placement of both radars and wind farms leads to high 2D-system performance measure values, corresponding to high air surveillance quality.

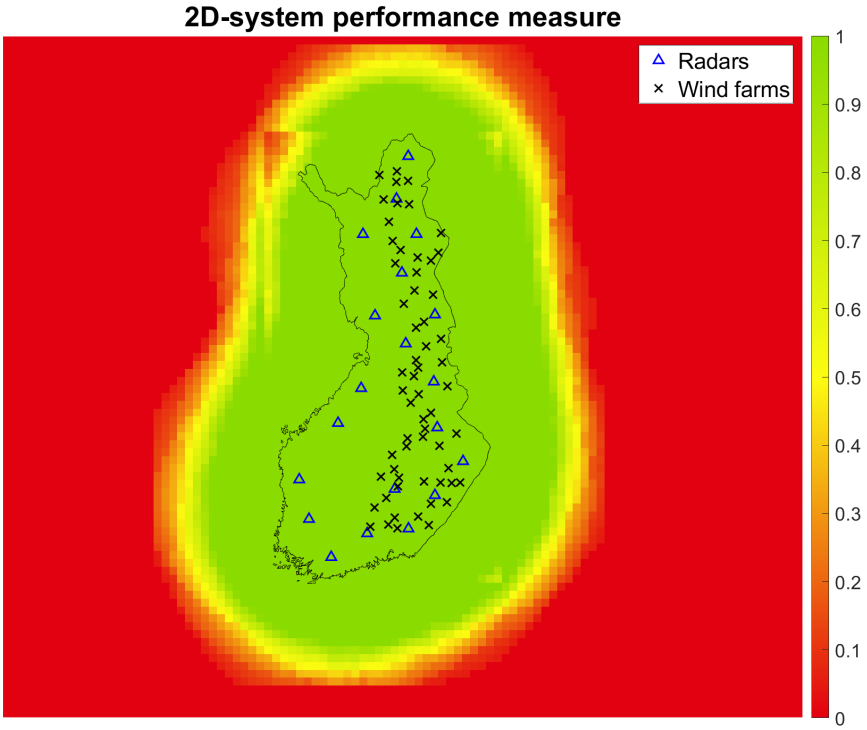

Figure 13: Optimal placement of radars and wind farms and the resulting 2D-system performance measure calculated with non-uniform weighting. The performance values are obtained with Equation 20, and are visualized without modification. The placements of radars and wind farms are purely fictitious and do not reflect any actual sites or development intentions.

The example problem is also solved with the 2D-formulation using uniform weighting, and the optimal placements and the 2D-system performance measure values are presented in Figure 14. Similar to the previous results, the radars are placed near the borders, and the wind farms are placed fairly evenly across the eastern region. The optimal radar system achieves high 2D-system performance measure values inland and in the surrounding area. In contrast to using the non-uniform weighting, there is no visible difference in the 2D-performance measure values between the inland and the surrounding areas, due to the uniform weighting. The value of the performance measure is at its maximum, value 1, in the entire inland area and near the borders. As discussed in Section 3.3.3, the overlapping coverage from multiple radars results in high 2D-system performance measure values for these areas.

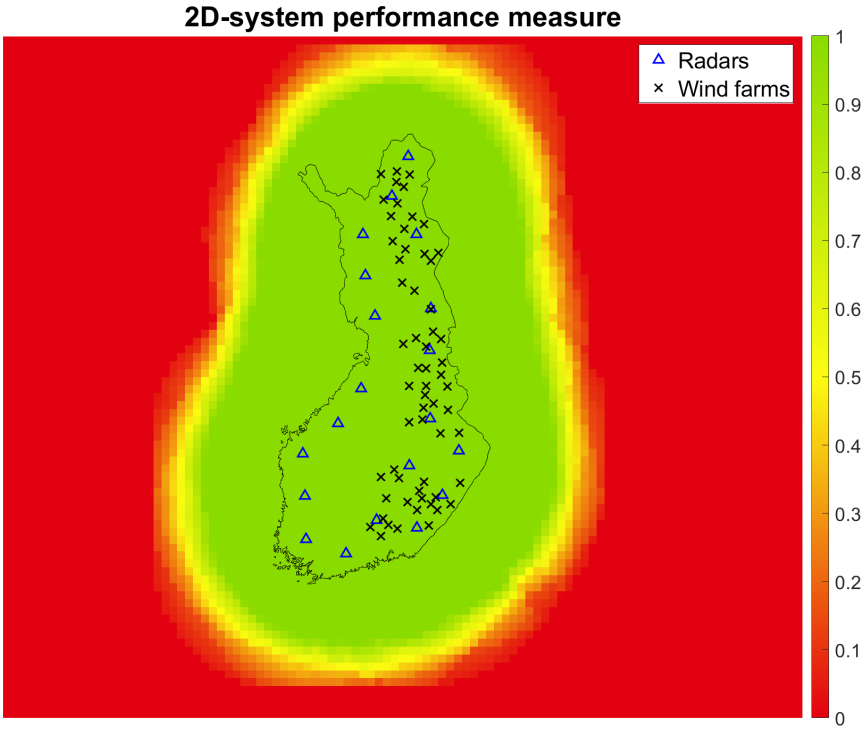

Figure 14: Optimal placement of radars and wind farms and the resulting 2D-system performance measure calculated with the uniform weighting. The performance values are obtained with Equation 20, and are visualized without modification. The placements of radars and wind farms are purely fictitious and do not reflect any actual sites or development intentions.

The adverse effect values resulting from the optimally placed wind farms are visualized in Figure 15 using both uniform and non-uniform weighting. The adverse effects using the non-uniform weighting are visualized on the left image, and using the uniform weighting in the right image. The color grading is constrained to the range $[0, 0.15]$, even though the adverse effect values can have values in the range $[0, 0.65]$. Similarly to the adverse effects with the 3D-formulation, the adverse effect values are higher with the non-uniform weighting, which is likely due to the higher weight given to the lower altitudes. With the uniform weighting, all the measurement points seem to have values less than 0.1. As discussed in Section 4.4.1, the values of the adverse effects are useful in comparing the wind farm placements. However, the objective is to maximize the 2D-system performance values, not minimize the adverse effect values. As the placements of the radar and the wind farms result in high 2D-system performance values with both weightings, i.e., to high air surveillance quality, the placements are good.

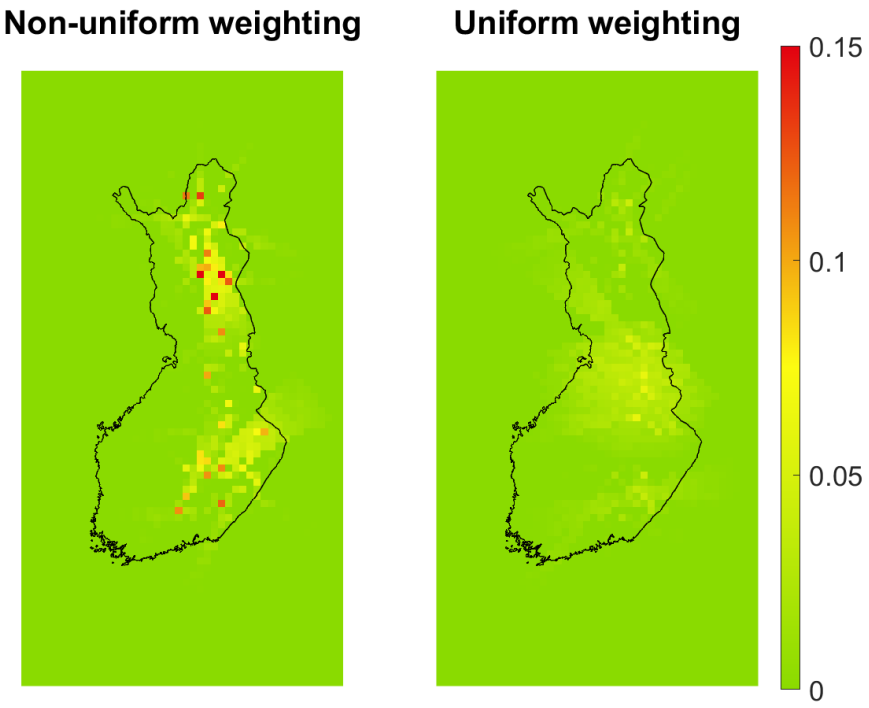

Figure 15: Adverse effects caused by the optimally placed wind farm on the radars.

4.4.3 Comparison

The 2D- and 3D-formulations differ in their computational complexity, which affects the amount of memory required and the solution time. In Table 3, the number of variables and constraints are presented, where a higher value corresponds to a higher complexity. Additionally, the solution time and required memory of the formulations and weightings are presented. The required memory is only for the performance matrix P and the adverse effect matrix A, and other variables used are not taken into consideration here.

The 3D-formulation was computationally more complex, with about 3 times as many variables and 1.7 times the number of constraints than the 2D-formulation, see Table 3. The optimization lasted on average 9 times longer than with the 2D-formulation, and required almost 10 times the memory. However, the example problem was solved in less than 6 minutes even with the 3D-formulation, which is reasonable for an optimization problem of this level of complexity. The solution time of the optimization varied between weightings.

The 3D-formulation with uniform weighting took around 1.3 times longer to solve than with the non-uniform weighting. With the 2D-formulation, the optimization took around 1.5 times longer with the non-uniform weighting. As the weighting directly affects the objective function, it also affects how the used optimization algorithm explores the solution space and thus the solution time. However, in this example, the difference in solution time was not significant in practical terms as the time differences with different weightings was less than two minutes.

In terms of memory requirements, the 3D-formulations required 10 times more

memory than the 2D-formulation. However, the matrices P_{3D} and A_{3D} were 19 times larger than the P_{2D} and A_{2D}. The size of the matrices did not linearly correspond to the amount of required memory due to sparse matrices being used. Such matrices only require memory for entries with nonzero values, which decreases the amount of memory used significantly. The use of sparse matrices was crucial, as the matrix A_{3D} had dimensions 71339×165034. If stored as a full dense matrix with double precision, i.e., 8 bytes per entry, it would require over 94 GB of memory, which is infeasible for the available computational resources. With the sparse matrices, the combined memory usage of P_{3D} and A_{3D} is only 75.8 MB, which is less than one-thousandth the size of 94 GB.

Table 3: Comparison of optimization formulations and weightings in terms of number of variables and constraints, amount of memory required, and the solution time

Formulation	Weighting	Number of variables	Number of constraints	Memory	Solution time
3D	Non-uniform	237 156	379 053	75.8 MB	355 s
3D	Uniform	237 156	379 053	75.8 MB	272 s
2D	Non-uniform	80 808	222 705	7.8 MB	42 s
2D	Uniform	80 808	222 705	7.8 MB	28 s

In Figure 16, the optimal placement of the radars obtained with different weightings is presented. The red triangles indicate radar placements that are optimal with both the uniform and non-uniform weightings. The yellow triangle indicates radar sites, which are only optimal using the non-uniform weighting, and the purple triangles indicate radar sites, which are optimal using the uniform weighting. In Figure 16, the left image presents the differences with the 3D-formulations, and the right image shows the differences with the 2D-formulations. The optimal solutions with the 2D- and 3D-formulations contain radar sites, which are optimal with both of the weightings. In the 3D-formulation, the radar sites in the southwestern side in spatial area 1 are all the same, as well as some sites in areas 5, 6, and 8. The 2D-formulation contains fewer shared radar sites, as more sites are slightly different between the weightings. This slight difference is evident in the spatial areas 1 and 7 of the 2D-formulation, where the sites are close to each other but not the same. These slight differences are also present in the 3D-formulation. The radar placements differ due to the non-uniform weighting placing higher weight on the eastern areas. This weight difference causes the radars to be placed such that the focus of the air surveillance is more to the east. Thus, the radars are placed further east. The shift in focus is implied in Figure 16, where the yellow triangles are placed slightly more to the east than the purple triangles. This shift is increasingly evident in the northern region, area 6, where the optimal radar site is placed significantly more east with non-uniform weighting. This larger shift is present in both the 2D- and 3D-formulations.

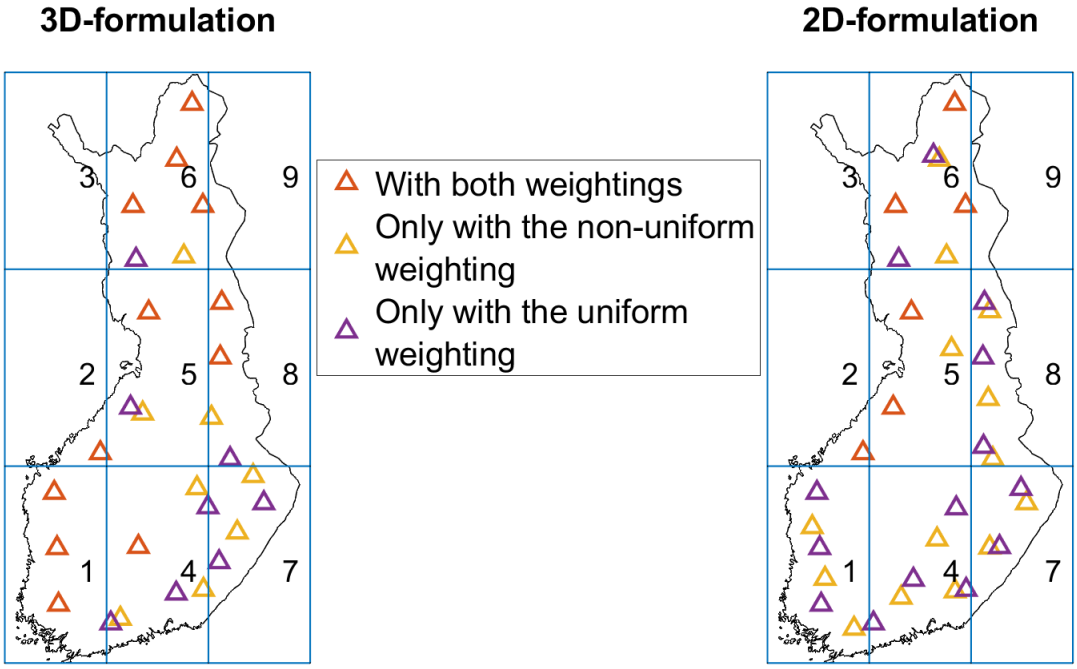

Figure 16: Comparison of the non-uniform and uniform weightings on the optimal radar placement, solved with the 3D- and 2D-formulations. Red triangles indicate radar sites selected with both non-uniform and uniform weightings. Yellow triangles are radar sites that are only optimal with the non-uniform weighting, and purple triangles are sites that are only optimal with uniform weighting. The placement of radars are purely fictitious and do not reflect any actual sites or plans.

The differences in the optimal radar placements between the optimization formulations is presented in Figure 17. The differences in the optimal placements with the 2D- and 3D-formulation and the non-uniform weighting is presented in the left image, and the differences with the uniform weighting in the right image. The radar placements which are optimal with both formulations are visualized with red triangles, the radar sites optimal only with the 3D-formulation are visualized with yellow triangles, and the radar sites optimal only with the 2D-formulation are visualized with purple triangles. With both weightings, multiple radar sites are shared by the optimal solution of both formulations, which can be seen by the number of red triangles. For example in the Lapland region, all but one radar site are optimal with both formulations with the non-uniform weighting. With the uniform weighting, even greater number of radar sites are shared between the formulations. With this weighting, all the radars sites on the western side, corresponding to areas 1,2, and 5, are optimal with both formulations. The optimal radar sites are more affected by the used formulation when the non-uniform weighting is used, as it has significantly less shared optimal radar sites compared to using uniform weighting. The difference in the optimal radar placements between formulations is likely caused by the effect of measurement points covered by multiple radars having higher performance values with the 2D-formulation than with the 3D-formulation. Due to this effect, radars can be placed more sparsely in areas with overlapping coverage. This effect can be observed in the example, as the

radars with the 2D-formulation leave larger gaps in the inland areas and still receive the highest possible 2D-system performance measure values. With both weightings, in area 4, the optimal radar sites with the 3D-formulation are closer to the center region of Finland than with the 2D-formulation. Aside from this difference, the radars are placed fairly similarly regardless of the formulation, and the radar sites, which were only optimal with the 2D-formulation, are typically close to the radars sites, which were only optimal with the 3D-formulation, and vice versa.

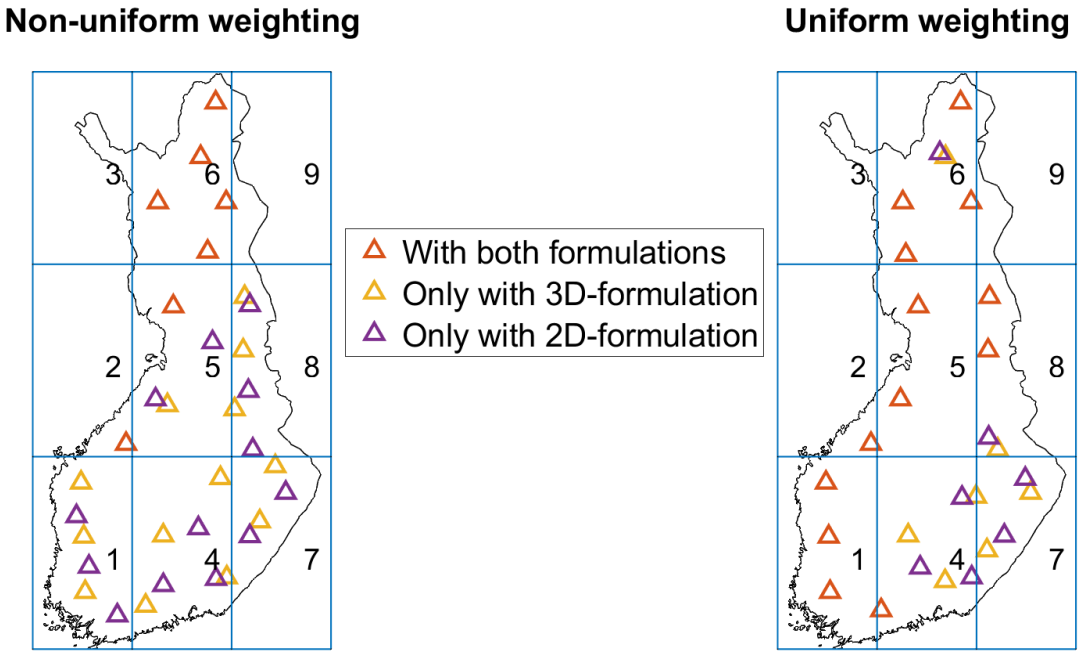

Figure 17: Comparison of the 2D- and 3D-formulations on the optimal radar placement, solved with the non-uniform and uniform weighting. Red triangles indicate radar sites selected in both the 2D- and the 3D-formulations. Yellow triangles refer to the radar sites which are only optimal with the 3D-formulation, and purple triangles to sites which are only optimal with the 2D-formulation. The placement of radars are purely fictitious and do not reflect any actual sites or plans.

5 Discussion

This section provides a discussion of the method developed for the joint placement of radars and wind farms. The key findings and limitations of the method are examined, and directions for future work are outlined. In addition, the results of the example problem are analyzed in more depth, discussing their interpretation and implications for practical application.

5.1 Findings

The example problem, presented in Section 4, demonstrated the capabilities of the placement method of radars and wind farms developed in this thesis. In the example, the number of placement options for radars is around $2 \cdot 10^{31}$ and the number of wind farm placement options $4 \cdot 10^{80}$. Therefore, the total number of radar-wind farm placement combinations is over 10^{100}. The additional constraints set on the placements, i.e., the distances between the radars and the wind farms, as well as the regional demand of wind farms in the North, Middle, and South regions, decrease the number of viable placement combinations. However, even with these additional constraints, the number of combinations is extremely large, which demonstrates the feasible size of the placement problem and the complexity of the optimization formulations. The optimization converged to a global optimum in minutes with both 2D- and 3D-formulations and weightings. The solution times additionally highlight the efficiency of the method, as the fastest solution was found in around 30 seconds, and the slowest in less than 6 minutes. The optimal placements in the example can be seen to be sensible in terms of air surveillance, as the radars are placed evenly all over the area of interest and the placements result in good air surveillance quality in the inland and outer areas.

In this thesis, two optimization formulations are derived. With the 3D-formulation, the air surveillance quality is evaluated at individual 3D-measurement points, which cover the area of interest. This evaluation at individual measurement points provides an accurate estimation of the air surveillance quality. However, the number of measurement points affects the computational complexity of the optimization. When the number of 3D-measurement points grows too large, the placement optimization with the 3D-formulation can become infeasible, meaning the optimization does not converge in a feasible amount of time. The 2D-formulation uses an aggregated performance measure, which decreases the number of measurement points and computational complexity. This aggregation reduces the accuracy of the air surveillance quality model, which affects the optimal placements of radars and wind farms. The example problem demonstrated that both formulations remain feasible even with a large number of placement options and measurement points. As mentioned above, the example problem converged to a global optimum in less than 6 minutes with the 3D-formulation and in less than 1 minute with the 2D-formulation. With both formulations, optimal placements for radars and wind farms are found, such that their respective system performance measures are maximized. The radar and wind farm placements result in high air surveillance quality, where the wind farms do not cause a visible reduction

in the air surveillance quality. The radars and wind farms are placed such that the adverse effects to the radars are minimal and the areas with adverse effects have overlapping coverage from multiple radars. The 2D- and 3D-formulations produce different optimal placements, which can be observed in Figure 17. However, the optimal radar placements are similar with both formulations. The radars are placed evenly near the border encircling the inland area, with some radars placed in the central regions of this area. Additionally, multiple radar sites are optimal with both formulations. The sites chosen only with the 2D-formulation are generally located very close to those chosen with the 3D-formulation. These similarities imply that the 2D-formulation provides a good approximation for the more accurate 3D-formulation. Moreover, because the optimal radar sites with the 2D-formulation are near the sites with the 3D-formulation, the radar coverages from these sites overlap extensively. Therefore, in practical terms, it may make little difference which formulation is used.

The modularity of the method allows for the individual components – such as the radar performance model, a wind farm effect model, or optimization formulations – to be modified without altering the remaining components. Therefore, the method provides a foundation for a large-scale joint placement optimization of radars and wind farms, which can be modified and expanded upon in future work.

5.2 Limitations

The method has its limitations, which affect its usability and the accuracy of solutions. These limitations originate partly from the scope of this thesis and partly due to the nature of the topic.

The radar performance model and the wind farm adverse effect model developed in this thesis are constructed purely based on fundamental physical principles and expert opinions from radar technology specialists. These models were appropriate for the scope of this thesis and for demonstrating the use of the placement method. However, these models have not been validated through comparison with real-world or simulated data to confirm their accuracy. Without validation, the usability of the method for real-world placement planning is limited.

The performance of radars is modeled with a gradual coverage model, which is a considerable simplification of air surveillance quality metrics, such as probability of detection and track performance. The use of these more developed metrics would improve modeling accuracy. However, they are computationally more demanding, which makes them impractical for large-scale placement optimization. The air surveillance quality is calculated as the sum of the radar performances. This summation does not account for effects such as diminishing returns from overlapping coverage, which can result in overestimating the surveillance quality. Additionally, the air surveillance quality is represented as a value between 0 and 1, and is solely based on distance to radars and wind farm interference. In reality, the air surveillance quality is dependent on a wide variety of factors and surveillance objectives. These objectives and factors could be formalized into air surveillance requirements, which indicate how accurately different target objects are required to be detected and tracked. The fulfillment of these air surveillance requirements determines the air surveillance

quality. However, this sort of surveillance objective formalization is not addressed in this thesis.

In the method, only one type of radar is used. This is unrealistic for real air surveillance systems, which consist of multiple types of radars, such as passive or multistatic radars. The radars typically vary in performance characteristics such as range, resolution, and update rate. Therefore, the method requires further development in placing different types of radars before it can be applied for supporting the planning of actual air surveillance systems.

In the example problem, the optimal placements of radars and wind farms are obtained with both formulations and with both weightings. These optimal placements maximize the total air surveillance quality in the area of interest. However, these placements are only optimal with respect to a specific problem, i.e., with the specific weighting and the number of wind farms and radars. Therefore, if the relative importance of some spatial areas or altitude ranges change – and thus the weighting – the optimal placements are likely to change as well. Such a placement change is not an issue for some radars, as they are designed to be movable. However, once wind farms are constructed, they cannot be relocated. Therefore, when planning the real-world wind farm placements, it is important to account for potential changes in the relative importance of spatial areas and altitude ranges. Similarly, the number of wind farms affects their optimal placements. As a result, placing wind farms sequentially – i.e., one at a time – is likely to generate less optimal solutions than determining locations for multiple new wind farms simultaneously. Therefore, the method is most suitable for long-term planning of multiple wind farm sites, rather than for individual projects.

5.3 Future work

The method developed in this thesis provides a foundation for the joint placement optimization of radars and wind farms. Relative to the example problem presented in Section 4, this method is capable of addressing larger-scale problems, encompassing larger geographic areas, a greater number of radars and wind farms, or finer spatial resolution, without requiring modification.

To confirm that the radar performance and adverse effect models presented in this thesis reliably represent real-world radar behavior and wind farm interference, validation of these models is required. Field testing could involve collecting data on how the performance of real-world radars decreases with distance and comparing it to predictions from the radar performance model. Similarly, the adverse effects of wind farms can be assessed by measuring the actual impact of existing wind farms on air surveillance quality and comparing these observations to the effects predicted by the adverse effect model. In a similar manner, computational validation can be carried out by comparing the radar performance and wind farm adverse effect estimates obtained from computational tools with the corresponding predictions of the models developed in this thesis. Such validation serves to confirm the accuracy of the models, increase confidence in their predictions, or adjust the models to enhance their fidelity. As the performances of the radars and the adverse effects of the wind farms are precomputed before the optimization, possible modifications to the performance models motivated

by validation results should not affect the efficiency of the optimization.

In the method, only monostatic radars are used, with a fixed range of 300 km. Typically, real-world air surveillance systems consist of different types of radars with different performance characteristics, such as range and resolution. Different radar types, such as passive radars or active electrically scanned array (AESA) radars (Richards et al., 2010), could also be considered in addition to the current monostatic ones. The different radar performance capabilities, such as varying ranges and time between observations, could also be taken into account. Similarly, only one type of wind farm is considered in this thesis. Wind farms can differ in size, orientation, and layout. These differences could be further addressed in the placement optimization. Additionally, the wind farms, which are already in operation or being constructed, should be taken into consideration in the placement optimization as these can affect the placement of the new wind farms.

In this thesis, the radar performance is described as a gradual coverage, where the air surveillance quality is the sum of the radar performance values. Both the radar performance and air surveillance quality metrics can be refined for greater accuracy. In the radar performance model, the probability of detection and the track accuracy could be explicitly estimated. The probability of detection can be modeled with a gradual coverage model of values between 0 and 1. This value can be combined from multiple radars to create a single detection probability at every measurement point. Track accuracy is typically estimated with simulation-based models (e.g., Brookner, 1998), which are infeasible for large-scale optimization. Therefore, an approximate model needs to be developed for the track accuracy. This approximate model could be used to make an estimate of the track accuracy at every measurement point, and this estimate would depend on the number of radars covering the point, their probability of detection, and the angles between the point and the radars. The angles between the measurement point and the radars affects how well a target's position can be triangulated. The track accuracy is reduced when the radars' LOSs are parallel, and improved as the LOSs become more perpendicular. In the future, the air surveillance quality could be determined as a combination of the detection probability and the track accuracy.

The overall goal in this thesis was to identify the radar and wind farm placement options that maximize the total air surveillance quality in the area of interest. These placement options have been determined by their respective planner, i.e., air surveillance planners or wind farm developers. The viability of a placement is dependent on multiple factors, such as distance to infrastructure and the cost of installation. Even though every placement option is viable, the placements can still differ in suitability or cost, making some placements more preferable to the planners. Currently, this preference information over the placement options is not considered in the placement method. In future work, the placement optimization could be formulated as a multi-criteria optimization problem, which would also consider criteria concerning the placement options, such as costs, in addition to air surveillance quality.

Developing the placement method to consider multiple criteria, use multiple radar types, or use more refined performance models increase the complexity of the optimization. As the complexity increases, the optimization can become infeasible to

solve. However, the example problem was solved in a fairly short time with only a commercial laptop. This demonstrates that the complexity can be increased even further while maintaining feasibility with the currently available computational resources. Furthermore, the used optimization software, Gurobi, allows for high-performance computing, meaning supercomputers that have significantly more computing power to be used. Increasing the computational resources allows for increasing the model complexity while maintaining feasibility of the optimization problem. Therefore, the proposed developments are unlikely to make the placement problem computationally infeasible.

The method developed in this thesis is able to consider differences in the importance of spatial areas and altitude ranges with weighting. The effect of the weighting is demonstrated by comparing two different weightings in the example problem. However, a more detailed analysis is needed to assess how sensitive the optimal placements are to changes in the weighting. In addition to a better understanding of the effects of weighting, this analysis can be used to determine robust placements for radars and wind farms, which remain optimal even with different weightings. Such robust placements are important to identify as the weighting can change over time. The weighting may change when the relative importance of spatial areas or altitude ranges shifts, e.g., due to new infrastructure developments or the introduction of new targets, such as drones. Especially with wind farms, which cannot be relocated once constructed, their robust placement can ensure that the site remains optimal even when the air surveillance priorities shift.

In this thesis, weights of spatial areas and altitude ranges are elicited with the centroid-weights method. The centroid-weights method only considers the ordinal importance information, meaning that only the rank order of the importance matters and not the actual importance differences. However, alternative weighting methods, such as SMART (Edwards & Barron, 1994) and Swing (Von Winterfeldt & Edwards, 1986), that use cardinal importance information could also be used. These methods consider the magnitude of the importance in addition to the rank order. With the SMART method, the importance of each spatial area and altitude range is rated, and these ratings are normalized to produce the weights. In the Swing method, spatial areas and altitudes are first ranked from worst to best, after which the relative additional value of improving air surveillance quality in the next-ranked area or altitude range is assessed sequentially. These weighting methods would likely produce different weights compared to the current weighting method, which affects the optimal solutions. In future work, the use of alternative weight elicitation methods could help verify that the chosen weights accurately reflect the relative importance of the spatial areas and altitude ranges. Additionally, instead of determining exact weights, a potential direction for future research could involve incorporating incomplete preference information (e.g., Harju et al., 2019; Mattila and Virtanen, 2015; Kokkala et al., 2019) into the placement method.

In this thesis, the spatial weight of an area is converted into a point-wise weight by dividing the area weight by the number of measurement points it contains. Therefore, the size of the spatial area affects the resulting weight of its measurement points. As discussed in Section 4.1, the spatial areas in the example problem vary significantly in

size. This difference in size means that higher spatial priority does not necessarily imply that the weight of a measurement point is higher. Differences in the area sizes can cause vagueness and confusion in determining the priorities and in interpreting the weights. To avoid such confusion, the spatial areas should be made roughly similar sizes. However, the areas in the example problem were sufficient in demonstrating the weighting and its effects.

The placement method developed in this thesis is able to identify good placements from a large set of placement options. However, the accuracy of this method is limited as the method uses simplified surveillance quality measures. The existing methods for comparing radar and wind farm placements (e.g., Lahti, 2022 and Hagnäs, 2025) are based on more accurate simulation-based modeling, but such modeling limits the number of placement options considered. In the future, the placement method could be used first to identify a set of good radar and wind farm sites from a large set of placement options. Then, these sites could be further analyzed with the more accurate simulation-based air surveillance evaluation methods, as the number of placement options to be considered has been decreased significantly.

6 Conclusions

This thesis considered the coexistence of radars and wind farms. The wind farms cause adverse effects on radars and decrease the air surveillance quality in the affected region. Both the severity of the adverse effects and the air surveillance quality are directly affected by the placement of the radars and the wind farms. The optimization of these placements enables the development of new wind farms while maintaining high air surveillance quality. Although some studies address the joint placement of radars and wind farms, existing methods are limited by computationally intensive simulations and cannot handle a large number of placement options. This thesis addressed this gap by developing a computationally efficient method for evaluating the performance of radars, estimating the adverse effects of wind farms, and optimizing their placements to maximize the air surveillance quality.

The optimization method for the placement of radars and wind farms was developed using mixed-integer linear programming. This method incorporates a radar performance model, which estimates the radar's capability to detect and track targets, and a wind farm adverse effect model, which describes how the performance of a radar is decreased by its interference with a wind farm. Based on these models, two system performance measures were developed to evaluate the resulting air surveillance quality from a combination of placed radars and wind farms. These measures differ on how accurately they can represent the air surveillance quality and in their computational complexity. The measures were used as a basis 2D and 3D optimization formulations. Similarly to the performance measures, these formulations differ in their computational complexity and accuracy. The 2D-formulation is computationally less complex than the 3D-formulation. However, the 2D-formulation uses an aggregated 2D-performance measure, producing less accurate results compared to the non-aggregated 3D-measure. The 3D-formulation uses this 3D-measure, which enables more accurate representation of the air surveillance quality. By using the non-aggregated measure, the computational complexity of the optimization problem is higher and takes longer to solve. However, even with the higher complexity, the 3D-formulation remains feasible even for large-scale problems with large number of placement options. The placement method is modular, meaning the individual components can be modified or replaced without changes to the entire method. The modular design allows for future enhancements, such as incorporating more sophisticated performance models or using alternative planning objectives.

The efficiency of the placement method introduced in this thesis and the feasible scale of placement problems were analyzed with an example problem involving over 10^{100} possible combinations of radar and wind farm placements. The solutions of the example problem converged to global optimum within minutes with both optimization formulations, demonstrating the computational efficiency. In the existing literature, no other method has demonstrated the ability to solve the joint placement of radars and wind farms at this scale while achieving both global optimality and a short runtime. The existing methods for this problem allow for more accurate modeling, but they cannot handle a large number of placement options because they are based on computationally heavy simulations. The new placement method enables the identification of radar and

wind farm sites that result in high-quality air surveillance when a large number of placement options is used. These sites could then be examined in more detail with the simulation-based models for increased air surveillance and adverse effect modeling accuracy.

The results of this thesis have clear practical implications. The placement method allows air surveillance planners and decision makers to make informed siting decisions by systematically exploring a large number of placement options and optimizing the radar and wind farm locations. The method can accelerate the planning of wind energy projects while maintaining high air surveillance quality, which supports both renewable energy and surveillance goals.

References

Abdelsalam, A. M., & El-Shorbagy, M. (2018). Optimization of wind turbines siting in a wind farm using genetic algorithm based local search. *Renewable Energy*, *123*, 748–755. https://doi.org/10.1016/j.renene.2018.02.083

Ahn, B. S. (2011). Compatible weighting method with rank order centroid: Maximum entropy ordered weighted averaging approach. *European Journal of Operational Research*, *212*(3), 552–559. https://doi.org/10.1016/j.ejor.2011.02.017

Baek, K.-H., Lee, Y., & Jang, H. (2014). Study on the optimal location of low altitude air defense radar. *Journal of the Korea Institute of Military Science and Technology*, *17*(2), 248–257. https://doi.org/10.9766/KIMST.2014.17.2.248

Bandaru, S., & Deb, K. (2016). Metaheuristic techniques. In *Decision sciences* (pp. 709–766). CRC Press.

Berman, O., Drezner, Z., & Krass, D. (2010). Generalized coverage: New developments in covering location models. *Computers & Operations Research*, *37*(10), 1675–1687. https://doi.org/10.1016/j.cor.2009.11.003

Blum, C., & Roli, A. (2003). Metaheuristics in combinatorial optimization: Overview and conceptual comparison. *ACM computing surveys (CSUR)*, *35*(3), 268–308. https://doi.org/10.1145/937503.937505

Borely, M. (2014). Guidelines on assessing the potential impact of wind turbines on surveillance sensors (1.2). https://www.eurocontrol.int/publication/eurocontrol-guidelines-assessing-potential-impact-wind-turbines-surveillance-sensors

Borges, C. L., & Falcão, D. M. (2006). Optimal distributed generation allocation for reliability, losses, and voltage improvement. *International Journal of Electrical Power & Energy Systems*, *28*(6), 413–420. https://doi.org/10.1016/j.ijepes.2006.02.003

Boudjemaa, R., & Oliva, D. (2019). A multi-objective approach to weather radar network architecture. *Soft Computing*, *23*(12), 4221–4238. https://doi.org/10.1007/s00500-018-3072-6

Brigada, D. J., & Ryvkina, J. (2021). Radar-optimized wind turbine siting. *IEEE transactions on sustainable energy*, *13*(1), 403–413. https://doi.org/10.1109/TSTE.2021.3113868

Brookner, E. (1998). *Tracking and kalman filtering made easy*. Wiley New York. https://doi.org/10.1002/0471224197

Capraro, G. T., Farina, A., Griffiths, H., & Wicks, M. C. (2006). Knowledge-based radar signal and data processing: A tutorial review. *IEEE Signal Processing Magazine*, *23*(1), 18–29.

Cetinay, H., Kuipers, F. A., & Guven, A. N. (2017). Optimal siting and sizing of wind farms. *Renewable Energy*, *101*, 51–58. https://doi.org/10.1016/j.renene.2016.08.008

Chemyak, V. (1998). *Fundamentals of multisite radar systems*. Routledge. https://doi.org/10.1201/9780203755228

Chen, W. K. (2004). *The electrical engineering handbook*. Academic Press.

Costanzo, G., Brindley, G., & Tardieu, P. (2025, February). Wind energy in europe: 2024 statistics and the outlook for 2025-2030 (R. O'Sullivan, Ed.). *WindEurope*. Retrieved August 23, 2025, from https://windeurope.org/intelligence-platform/product/wind-energy-in-europe-2024-statistics-and-the-outlook-for-2025-2030/

Cranmer, A., Baker, E., Liesiö, J., & Salo, A. (2018). A portfolio model for siting offshore wind farms with economic and environmental objectives. *European Journal of Operational Research*, *267*(1), 304–314. https://doi.org/10.1016/j.ejor.2017.11.026

Curry, G. R. (2004). *Radar system performance modeling* (2nd ed.). Artech.

Drezner, Z., Wesolowsky, G. O., & Drezner, T. (2004). The gradual covering problem. *Naval Research Logistics (NRL)*, *51*(6), 841–855. https://doi.org/10.1002/nav.20030

Edwards, W., & Barron, F. H. (1994). Smarts and smarter: Improved simple methods for multiattribute utility measurement. *Organizational behavior and human decision processes*, *60*(3), 306–325. https://doi.org/10.1006/obhd.1994.1087

European Commission. (2023, October). *European wind power action plan* (tech. rep. No. COM/2023/669 final). https://eur-lex.europa.eu/legal-content/EN/TXT/?uri=CELEX:52023DC0669

Finnish Air Force. (n.d.). *Ilmavalvontatutkat ovat alueellisen koskemattomuuden valvonnan perustyökaluja*. Retrieved July 18, 2025, from https://ilmavoimat.fi/ilmavalvontatutkat_vanha

Freeman, R. L. (2007). *Radio system design for telecommunications*. John Wiley & Sons.

Garey, M. R., & Johnson, D. S. (1979). *Computers and intractability: A guide to the theory of np-completeness*. W. H. Freeman.

Gilbert, J. R., Moler, C., & Schreiber, R. (1992). Sparse matrices in matlab: Design and implementation. *SIAM Journal on Matrix Analysis and Applications*, *13*(1), 333–356. https://doi.org/10.1137/0613024

Godrich, H., Petropulu, A. P., & Poor, H. V. (2011). Sensor selection in distributed multiple-radar architectures for localization: A knapsack problem formulation. *IEEE Transactions on Signal Processing*, *60*(1), 247–260. https://doi.org/10.1109/TSP.2011.2170170

Hagnäs, R. (2025). *Optimization of radar and wind farm placement using computationally intensive simulations* [Master's thesis]. Aalto University. https://aaltodoc.aalto.fi/items/f4a06683-ec17-47f6-8b5e-03dc8a85b9f9

Harju, M., Liesiö, J., & Virtanen, K. (2019). Spatial multi-attribute decision analysis: Axiomatic foundations and incomplete preference information. *European Journal of Operational Research*, *275*(1), 167–181. https://doi.org/10.1016/j.ejor.2018.11.013

He, H., Daumé, H., & Eisner, J. (2014). Learning to search in branch and bound algorithms. In Z. Ghahramani, M. Welling, C. Cortes, N. Lawrence, & K. Weinberger (Eds.), *Advances in neural information processing systems* (Vol. 27). Curran Associates, Inc.

Hochbaum, D. S. (2007). Complexity and algorithms for nonlinear optimization problems. *Annals of Operations Research*, *153*(1), 257–296.

Huang, H.-S. (2007). Distributed genetic algorithm for optimization of wind farm annual profits. *2007 International Conference on Intelligent Systems Applications to Power Systems*, 1–6. https://doi.org/10.1109/ISAP.2007.4441654

Joensuu, K., Väyrynen, L., Tolppanen, J., Karhu, L., Salmi, T., Hartikka, S., Leino, L., Viljanen, J., Smids, S., Hujanen, A., et al. (2021). Tuulivoimarakentamisen edistäminen: Keinoja sujuvaan hankekehitykseen ja eri tavoitteiden yhteensovitukseen. *Valtioneuvosto*. http://urn.fi/URN:ISBN:978-952-383-354-8

Kennedy, J., & Eberhart, R. (1995). Particle swarm optimization. *Proceedings of ICNN'95-international conference on neural networks*, *4*, 1942–1948. https://doi.org/10.1109/ICNN.1995.488968

Keränen, T. (2020, July). Kiinteät keskivalvontatutkat hyvästeltiin upinniemen ja kaamasen tutka-asemilla. *Ruotuväki*. Retrieved August 20, 2025, from https://ruotuvaki.fi/-/kiinteat-keskivalvontatutkat-hyvasteltiin-upinniemen-ja-kaamasen-tutka-asemilla

Kim, M.-G., & Dalhoff, P. H. (2014). Yaw systems for wind turbines – overview of concepts, current challenges and design methods. *Journal of Physics: Conference Series*, *524*(1), 012086. https://doi.org/10.1088/1742-6596/524/1/012086

Knott, E. F., Schaeffer, J. F., & Tulley, M. T. (2004). *Radar cross section* (2nd ed.). SciTech Publishing.

Koch, T., Berthold, T., Pedersen, J., & Vanaret, C. (2022). Progress in mathematical programming solvers from 2001 to 2020. *EURO Journal on Computational Optimization*, *10*, 100031. https://doi.org/10.1016/j.ejco.2022.100031

Kokkala, J., Berg, K., Virtanen, K., & Poropudas, J. (2019). Rationalizable strategies in games with incomplete preferences. *Theory and Decision*, *86*(2), 185–204. https://doi.org/10.1007/s11238-018-9681-9

Lahti, P. (2022). *Compensation of adverse effects of wind farms on air surveillance capability using spatial decision analysis* [Master's thesis, Aalto University]. https://urn.fi/URN:NBN:fi:aalto-202206194062

Leijnse, H., Teschl, R., Paulitsch, H., Teschl, F., Holmes, G., & Sidselrud, L. F. (2022, August). *On the coexistence of weather radars and wind turbines* (tech. rep.). EUMETNET OPERA. Retrieved August 15, 2025, from https://www.eumetnet.eu/wp-content/uploads/2022/08/OPERA_wind_turbine_report_20220225.pdf

Lemmon, J. J., Carroll, J. E., Sanders, F. H., & Turner, D. (2008, July). *Assessment of the effects of wind turbines on air traffic control radars* (tech. rep. No. TR-08-454). US Department of Commerce.

Mattila, V., & Virtanen, K. (2015). Ranking and selection for multiple performance measures using incomplete preference information. *European Journal of Operational Research*, *242*(2), 568–579. https://doi.org/10.1016/j.ejor.2014.10.028

Merriam-Webster. (n.d.). *Air surveillance*. Retrieved July 17, 2025, from https://www.merriam-webster.com/dictionary/air%20surveillance

Norin, L., & Haase, G. (2012, April). Doppler weather radars and wind turbines. In *Doppler radar observations-weather radar, wind profiler, ionospheric radar, and other advanced applications* (pp. 333–354). InTech. https://doi.org/10.5772/39029

Olivier, B., Pierre, G., Nicolas, H., Loıc, O., Olivier, T., & Philippe, T. (2009). Multi sensor data fusion architectures for air traffic control applications. In *Sensor and data fusion*. IntechOpen. https://doi.org/10.5772/6573

Padberg, M. (2013). *Linear optimization and extensions* (Vol. 12). Springer Science & Business Media.

Peiponen, P. (2022, April). Maakuntajohtajat vaativat hyvitystä itärajan valvonnasta – itä-suomi jää paitsi paljon hehkutetusta tuulivoimasta venäjän läheisyyden vuoksi. Retrieved August 18, 2025, from https://yle.fi/a/3-12417048

Pelli, P. (2023, December). Hs ympäristö: Tuulivoima olisi itä-suomessa erityisen kannattavaa, jos sitä saisi rakentaa. *Helsingin Sanomat*. Retrieved August 20, 2025, from https://www.hs.fi/talous/art-2000010066395.html

Pertilä, P., Jylhä, J., Nissilä, J., & Väilä, M. (2023). Efficient fresnel diffraction for wind turbines. *2023 IEEE Conference on Antenna Measurements and Applications (CAMA)*, 693–697. https://doi.org/10.1109/CAMA57522.2023.10352896

Rekik, S., Khabbouchi, I., & El Alimi, S. (2025). A spatial analysis for optimal wind site selection from a sustainable supply-chain-management perspective. *Sustainability*, *17*(4), 1571. https://doi.org/10.3390/su17041571

Richards, M. A., Scheer, J., Holm, W. A., & Melvin, W. L. (2010). *Basic principles* (Vol. 1). SciTech Publishing.

Roy, U. K., & Acharya, S. (2017). Optimization of weather radar network using pso. *2017 IEEE 7th International Advance Computing Conference (IACC)*, 37–42. https://doi.org/10.1109/IACC.2017.0023

Ruotsalainen, M., & Jylhä, J. (2017). Learning of a tracker model from multi-radar data for performance prediction of air surveillance system. *2017 IEEE Congress on Evolutionary Computation (CEC)*, 2128–2136. https://doi.org/10.1109/CEC.2017.7969562

Saidur, R., Rahim, N. A., Islam, M. R., & Solangi, K. H. (2011). Environmental impact of wind energy. *Renewable and sustainable energy reviews*, *15*(5), 2423–2430. https://doi.org/10.1016/j.rser.2011.02.024

Simon, D. (2013). *Evolutionary optimization algorithms*. John Wiley & Sons.

Skolnik, M. I., et al. (1980). *Introduction to radar systems* (2nd ed., Vol. 3). McGraw-hill New York.

Tanergüçlü, T., Maraş, H., Gencer, C., & Aygüneş, H. (2012). A decision support system for locating weapon and radar positions in stationary point air defence. *Information Systems Frontiers*, *14*(2), 423–444. https://doi.org/10.1007/s10796-010-9269-6

Theil, A., Schouten, M. W., & de Jong, A. (2010). Radar and wind turbines: A guide to acceptance criteria. *2010 IEEE Radar Conference*, 1355–1361. https://doi.org/10.1109/RADAR.2010.5494405

Vanderbei, R. J. (2020). *Linear programming : Foundations and extensions* (5th ed. 2020.). Springer International Publishing.

Virtanen, M. (2024). *Evaluation of quality of air surveillance using spatial multi-criteria decision analysis* [Master's thesis, Aalto University]. https://urn.fi/URN:NBN:fi:aalto-202411217306

Von Winterfeldt, D., & Edwards, W. (1986). Decision analysis and behavioral research. *Cambridge University Press*.

Wang, B. (2010). *Coverage control in sensor networks*. Springer-Verlag. https://doi.org/10.1007/978-1-84996-059-5

Wimhurst, J. J., Nsude, C. C., & Greene, J. S. (2023). Standardizing the factors used in wind farm site suitability models: A review. *Heliyon*, *9*(5), e15903. https://doi.org/10.1016/j.heliyon.2023.e15903

Zohuri, B. (2020). *Radar energy warfare and the challenges of stealth technology*. Springer Cham. https://doi.org/10.1007/978-3-030-40619-6